การเตรียมเมมเบรนโลหะผสมแพลเลเดียม-คอปเปอร์-ซิลเวอร์บนเหล็กกล้าไร้สนิม

สำหรับการแยกไฮโดรเจน

นางสาว วรันต์ภรณ์ ภัทรธีรนนท์

ศูนย์วิทยทรัพยากร
จุฬาลงกรณ์มหาวิทยาลัย

วิทยานิพนธ์นี้เป็นส่วนหนึ่งของการศึกษาตามหลักสูตรปริญญาวิทยาศาสตรมหาบัณฑิต
สาขาวิชาปิโตรเคมีและวิทยาศาสตร์พอลิเมอร์
คณะวิทยาศาสตร์ จุฬาลงกรณ์มหาวิทยาลัย
ปีการศึกษา 2553

PREPARATION OF PALLADIUM-COPPER-SILVER ALLOY MEMBRANE ON STAINLESS STEEL FOR HYDROGEN SEPARATION

Miss.Warunporn Pattarateeranon

ศูนย์วิทยทรัพยากร
จุฬาลงกรณ์มหาวิทยาลัย

A Thesis Submitted in Partial Fulfillment of the Requirements

for the Degree of Master of Science Program in Petrochemistry and Polymer Science

Faculty of Science

Chulalongkorn University

Academic Year 2010

Thesis Title	PREPARATION OF PALLADIUM-COPPER-SILVER ALLOY MEMBRANE ON STAINLESS STEEL FOR HYDROGEN SEPARATION
By	Miss Warunporn Pattarateeranon
Field of Study	Petrochemistry and Polymer Science
Thesis Advisor	Assistant Professor Sukkaneste Tungasmita, Ph.D.
Thesis Co-adviser	Associate Professor Supawan Tantayanon, Ph.D.

Accepted by the Faculty of Science, Chulalongkorn University in Partial Fulfillment of the Requirements for the Master's Degree

....Dean of the Faculty of Science

(Professor Supot Hannongbua, Dr.rer.nat.)

THESIS COMMITTEE

....Chairman

(Professor Pattarapan Prasassarakich, Ph.D.)

....Thesis Adviser

(Assistant Professor Sukkaneste Tungasmita, Ph.D.)

....Thesis Co-adviser

(Associate Professor Supawan Tantayanon, Ph.D.)

....Examiner

(Associate Professor Wimonrat Trakarnpruk, Ph.D.)

....External Examiner

(Sutheerawat Samingprai, Ph.D.)

วรันต์ภรณ์ ภัทรธีรนนท์: การเตรียมเมมเบรนโลหะผสมแพลเลเดียม-คอปเปอร์-ซิล
เวอร์บนเหล็กกล้าไร้สนิมสำหรับการแยกไฮโดรเจน (PREPARATION OF Pd-Cu-
Ag ALLOY MEMBRANE ON STAINLESS STEEL FOR HYDROGEN
SEPARATION) อ.ที่ปรึกษาวิทยานิพนธ์หลัก: ผศ.ดร.สุคคเณศ ตุงคะสมิต, อ.ที่
ปรึกษาวิทยานิพนธ์ร่วม: รศ.ดร.ศุภวรรณ ตันตยานนท์, 86 หน้า.

การปรับปรุงและพัฒนาเมมเบรนโลหะผสมเทอนารีแพลเลเดียม-ซิลเวอร์-คอปเปอร์
บนตัวรองรับเหล็กกล้าไร้สนิมชนิด 316L สำหรับการแยกไฮโดรเจนที่เตรียมขึ้นด้วยเทคนิคการ
ชุบเคลือบแบบไม่ใช้กระแสไฟฟ้าและการชุบเคลือบแบบใช้ไฟฟ้า พบว่ามีโครงสร้างจุลภาคและ
การยึดเกาะของฟิล์มที่ดี ไม่พบผลที่เกิดจากความเปราะของไฮโดรเจนเมื่อใช้ในการแยก
ไฮโดรเจนที่อุณหภูมิใช้งาน อัตราส่วนของโลหะผสมแพลเลเดียม-ซิลเวอร์-คอปเปอร์ควบคุม
โดยเวลาในการชุบเคลือบและองค์ประกอบของโลหะสำหรับการเคลือบ ลักษณะพื้นผิว
องค์ประกอบและโครงสร้างของเฟสของเมมเบรนตรวจสอบโดยกล้องจุลทรรศน์อิเล็กตรอน
แบบส่องกราดที่ติดตั้งเครื่องวิเคราะห์ธาตุเชิงพลังงานและเครื่องวัดการเลี้ยวเบนรังสีเอ็กซ์
ตามลำดับ โครงสร้างของเฟสหลังจากการอบแสดงถึงองค์ประกอบของโลหะผสมแพลเลเดียม-
คอปเปอร์ แพลเลเดียม-ซิลเวอร์ และแพลเลเดียม-ซิลเวอร์-คอปเปอร์ ที่เกิดขึ้นและมีการ
กระจายตัวของโลหะแพลเลเดียม, คอปเปอร์และซิลเวอร์ที่สม่ำเสมอมากทั่วทั้งเมมเบรน
ปริมาณการแพร่ผ่านของไฮโดรเจนซึ่งวัดที่อุณหภูมิ 350-500 องศาเซลเซียส ที่ความดัน 1-3
บรรยากาศ ผลปรากฏว่ามีการแพร่ผ่านของไฮโดรเจนเพิ่มขึ้น เมื่อเพิ่มอุณหภูมิและความดัน
ปริมาณการแพร่ผ่านของไฮโดรเจนที่ได้จากแพลเลเดียมเมมเบรนที่มีชั้นกั้นการแพร่โครเมียม
ออกไซด์จะมีปริมาณสูงกว่าแบบเมมเบรนที่ไม่มีชั้นกั้นการแพร่ ไม่เพียงแต่ว่าเมมเบรนโลหะ
ผสมแพลเลเดียม-ซิลเวอร์-คอปเปอร์จะให้ปริมาณการแพร่ผ่านของไฮโดรเจนสูง แต่ยังมีสมบัติ
เชิงกลที่ดี ซึ่งสามารถป้องกันผลจากความเปราะเนื่องมาจากไฮโดรเจนได้อีกด้วย

สาขาวิชา	ปิโตรเคมีและวิทยาศาสตร์พอลิเมอร์	ลายมือชื่อนิสิต ___วรันต์ภรณ์ ภัทรธีรนนท์___
ปีการศึกษา	2553	ลายมือชื่อ อ.ที่ปรึกษาวิทยานิพนธ์หลัก___
		ลายมือชื่อ อ.ที่ปรึกษาวิทยานิพนธ์ร่วม___

5172435723 : MAJOR PETROCHEMISTRY AND POLYMER SCIENCE
KEYWORDS: Pd ALLOY MEMBRANE/ HYDROGEN SEPARATION/
ELECTROPLATING/ ELETROLESS PLATING/CROMIUM OXIDE

WARUNPORN PATTARATEERANON: PREPARATION OF Pd-Cu-Ag ALLOY MEMBRANE ON STAINLESS STEEL FOR HYDROGEN SEPARATION ADVISOR: ASST. PROF., SUKKANESTE TUNGASMITA, Ph.D., CO-ADVISOR: ASSOC. PROF. SUPAWAN TANTAYANON, Ph.D., 86 pp.

An improvement and developement of ternary Pd-Ag-Cu alloy membranes on 316L stainless steel substrates for hydrogen separation have been prepared by electroless and electroplating techniques. It was found that, the microstructure and adhesion of the films was good which the effects of hydrogen embrittlement cannot be observed when used in the hydrogen separation at working temperature. Pd-Ag-Cu alloy ratio was controlled by plating time and metal composition for plating. The surface morphology, composition and phase structures of the membrane were investigated by scanning electron microscope equipped with energy dispersive x-ray diffraction and X-ray diffractrometer, respectively. The phase structure after annealing indicated the alloy composition of Pd-Cu, Pd-Ag and Pd-Ag-Cu were formed with highly uniform distribution of Pd, Ag and Cu metal throughout of the membrane. The hydrogen permeation flux which was measured at 350-500°C in pressure differences of 1-3 atm. As a result, hydrogen permeance increased with operating temperature and pressure. The hydrogen permeation flux obtained from Pd membranes with the Cr_2O_3 as intermetallic diffusion barriers was higher than that without. Not only Pd-Ag-Cu alloy membrane has a high hydrogen permeance but also has a good mechanical property, which can prevent the hydrogen embrittlement.

Field of Study : <u>Petrochemistry and Polymer Science</u> Student's Signature Warunporn Pattarateeranon

Academic Year: <u>2010</u> Advisor's Signature Sukkaneste Tungasmita

Co-advisor's Signature

ACKNOWLEDGEMENTS

CONTENTS

LIST OF TABLES

LIST OF FIGURE

LIST OF ABBREVIATIONS

D	Diffusion coefficient (m^2s^{-1})
J	Diffusion Flux (atoms $m^{-2}s^{-1}$)
X	the distance (m)
XRD	X-ray diffraction
SEM	Scanning electron microscope
EDS	Energy dispersive spectrometer
Pd	Palladium
Ag	Silver
Cu	Copper
SS	Stainless steel
°C	Degree Celsius
g	Gram
eV	Electron volt
mL	Milliliter
min	Minute
h	Hour
cm	Centimeter
nm	Nanometer
μm	Micrometer

CHAPTER I

INTRODUCTION

1.1 Introduction

In these recent years, the demand for using hydrogen as a clean energy has increased rapidly and hydrogen is becoming one of the key energy resources of the future and is mainly used in the petrochemical industries and a small amount in fuel cell operation. The global hydrogen economy is worldwide research and development for low-cost production of hydrogen from hydrocarbons or water. One of the most effective ways to produce pure hydrogen is to use inorganic membranes for hydrogen separation and membrane reactor applications. These issues become more and more important and attractive to us because of the worldwide energy crisis and environment pollution. Hydrogen purification is an essential step in industrial hydrogen production and the latest in the succession as an energy carrier, with many social, economic and environmental benefits [1]. The increasing demand for highly pure hydrogen from a variety of feedstocks has driven a significant amount of research topics on the development of Pd membranes.

Many efforts have been made to develop new membrane materials with low cost and high performance for hydrogen permeability [2]. The high hydrogen permeability and chemical resistance make the Pd-based alloy membranes a high potential in hydrogen separation and membrane reactors. The material cost and hydrogen permeation rates can be optimized by using a thin layer of Pd coated on a highly hydrogen permeable substrates such as porous ceramics, metal oxides and metallic materials [3].

Porous substrates, such as porous stainless steel, have often been employed for Pd membrane because thermal expansion coefficient being close to that of Pd-based films, as well as the corrosion resistance, high thermal stability and good mechanical strength. Electroless and electroplating coating are two most popular methods for the synthesis of dense membranes. Currently membrane separation is one of the most cost-effective methods for high purity hydrogen production [4].

1.2 Pd alloys for improving hydrogen permeation flux and thermally stability

Pd-based alloys may have advantages over Pd for the use in hydrogen separation and membrane reactor applications. In some cases, the hydrogen permeability of alloys is greater than that of Pd. Several tertiary Pd-based alloys such as Pd-Ru-In, Pd-Ag-Ru and Pd-Ag-Rh reported to have high hydrogen permeability. Pd-based alloys may produce membranes with enhanced chemical resistance. To improve the hydrogen flux, other materials that have higher hydrogen permeability than Pd-Cu binary alloys, is needed to add into the alloy metric. The Pd-Ag-Cu alloys, which are studied in this research, has been proved to increase hydrogen permeability and could be a good candidate as membrane materials. Furthermore, mass-scale and cost-effective production of industrial scale Pd-based alloy thin film membranes need to be demonstrated to be competitive in the hydrogen production and purification [5]. Moreover, Pd-based alloy membranes have more advantages such as good mechanical properties, better resistance to hydrogen embrittlement, chemical compatibility and low cost. In the development of this ternary alloy, we have developed the alloys that would improve hydrogen permeability with a small amount of metal additive to Pd membrane.

1.3 Objective

- To carry out fundamental studies and control the preparation of a binary and ternary Pd-based alloy membrane for hydrogen separation.

1.4 Scope of research

- Prepare and characterize the Pd-Cu, Pd-Ag and Pd-Ag-Cu alloy membranes.
- Control the rate for plating and alloy compositions of Pd, Cu and Ag metallic elements on 316L stainless steel substrates.
- Characterize the hydrogen permeation rate of the alloy membrane.

CHAPTER II

THEORY AND LITERATURE REVIEWS

2.1 Pd Membranes

Recently many efforts focused on the hydrogen separation for fuel cell applications, which have been devoted to development of pure Pd and Pd-alloyed composite membrane [6]. The Pd holds a unique property among all the metallic elements in being able to take into solution large quantities of hydrogen while simultaneously retaining a high degree of ductility. These attributes coupled with the high mobility or high diffusion rate of hydrogen in the lattice, have been exploited in the use of Pd and subsequently of Pd-based alloys as a hydrogen diffusion/separation membranes. The hydrogen permeation in the Pd membrane has been extensively investigated using permeation methods [7].

For a pure Pd membrane, it has mainly been restricted because of phase transition from α to β phase. The phase transition occurs generally at temperatures below 300°C and pressure below 2×10^6 Pa, depending on the hydrogen concentration in the metal. Since the lattice constant of the β-phase is larger than the α-phase. The phase transition leads to lattice strain and distortion of the metal lattice, known as *embrittlement* [8].

The hydrogen embrittlement of pure Pd membrane can be overcomed by alloying the metallic Pd. The presence of metal group I-IV also enhances the hydrogen permeation flux with no detrimental effects on its selectivity [9]. Pd-alloys are typically operated at temperatures from 300-600°C and exhibit good mechanical properties. Although Pd-alloys have a higher permeability than other membrane materials but the achievable flux is often limited by the thickness of the metal films. Pd-based alloys especially with Cu and Ag, are the primary metals utilized due to their high surface reactivity for hydrogen dissociation, resistance to embrittlement, providing thermal stability, also increases resistance to chemical contaminants and high hydrogen permeability [10].

2.2 Hydrogen permeable membranes

Gas separation at high temperature is very attractive since many petrochemical processes could be enhanced by gas separation through the membrane at operating condition. Metal membrane made of Pd can be used to sieve hydrogen from mixed gas [11].
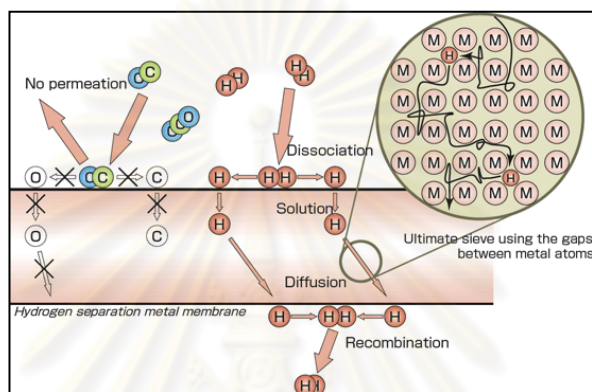
Figure 2.1 Principle of hydrogen separation through metal membrane [12].

As illustrated in Figure 2.1, the hydrogen permeation is inversely proportional to the thickness of the membrane thin film. On the other hand, thinner films have low mechanical strength and low selectivity at higher temperature [13]. These conditions always need to be compromised.
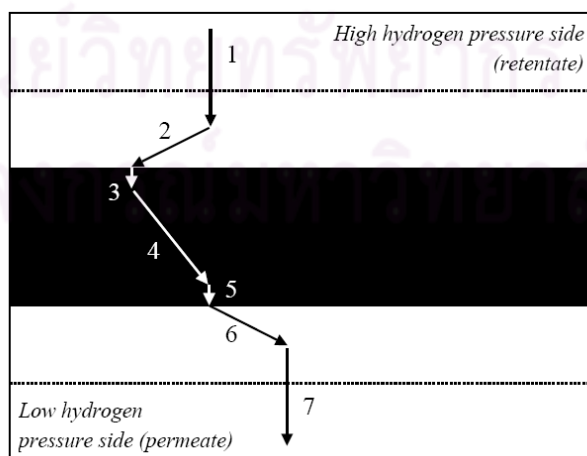
Figure 2.2 Schematic of hydrogen permeation mechanism in Pd membranes.

For the hydrogen diffusion through the membrane, as seen in Figure 2.2, the hydrogen diffusion occurs via a series of different steps:

(1) Diffusion of hydrogen to the metal surface.

(2) Adsorption of hydrogen on the surface.

(3) Splitting of hydrogen molecules and incorporation in to the metal.

(4) Diffusion of protons in the lattice and of electrons in the electron bands.

(5) Regeneration of hydrogen molecules on the permeated side surface.

(6) Desorption of the hydrogen molecules.

(7) Diffusion of the hydrogen molecules from the surface.

Assuming that the rate limiting step of hydrogen permeation is controlled by the hydrogen diffusion through the bulk Pd layer, the hydrogen flux can be expressed by the Fick's first law, [14]

$$J = -D\frac{dc}{dl} = \frac{D}{l}(C_{HP} - C_{LP})$$ (2.1)

In equation 2.1, J is the hydrogen permeation flux, in the unit of $m^3/m^2.s$ or $mol/m^2.s^{-1}$. D is the diffusivity of the hydrogen in the Pd membrane (m^2/s^1) and l is the thickness of the membrane (m). Subscripts HP and LP designate the high and low pressure sides of the membrane (mol/m^3). C is the hydrogen concentrations, which can be expressed as,

$$C = k\eta \quad [2]$$ (2.2)

where k is the concentration constant for hydrogen (mol/m^3) and η is the H/Pd atomic ratio. At very low concentrations of hydrogen, η is linearly dependent on the square root of the partial pressure of hydrogen, $C = kp^{1/2}$, a good approximation outside the immiscibility region. This reduces to

$$J = \frac{kD}{l}(P_{HP}^{1/2} - P_{LP}^{1/2})$$ (2.3)

Both k and D are functions of temperature and *the term kD* is the permeability. It is often difficult to determine the membrane thickness accurately. The value of P, which equal to kD/l($k.mole/m^2s.Pa^{1/2}$), defined as the permeance and frequently used. However, the exponent of the pressure is not 1/2 due to factors such as the non-

linearity of the $P^{1/2}$-C isotherm, surface reaction and existence of significant mass transfer resistances and diffusion through the Pd bulk. Therefore, equation 2.4 can be expressed in a general form as, [15]

$$J = P(P_{HP}^{n} - P_{LP}^{n})$$ (2.4)

where $1 \geq n \leq 1/2$, For the Sievert's law, $n = 1/2$.

2.3 Intermetallic diffusion of Pd membranes

The porous metal substrates are used at high temperatures the intermetallic diffusion of metal elements from the substrate to the Pd separation layer causes the hydrogen flux to deteriorate. One way to improve the membrane stability is to create an intermediate intermetallic diffusion barrier layer, which is stable at reducing atmosphere and at high temperatures [16].

The operation at high temperature can deteriorate the performance of the Pd membrane. As the porous stainless steel substrates were used for the operation temperatures above 400°C, interdiffusion of atomic metals between Pd-based membranes and substrate materials can be occurred. The important factor of intermetallic diffusion between Pd membranes and integral element of porous stainless steel substrates is the *Tamman temperature*. The Tamman temperature is the temperature of a metal which equals to one half of its melting point and the temperature at or above which its atomic vibration starts to be considerable. If the temperature was increased to 650°C or 923 K, a temperature higher than the Tamman temperature of 316L stainless steel (550°C 833K) and Pd (640°C or 913 K), intermetallic diffusion significantly took place with an apparent and continuous decline of hydrogen permeance, poor-selectivity and shorter-life Pd membrane. Nonetheless, intermetallic diffusion could be prevented by using a diffusion barrier to avoid direct contact of the Pd membranes with the stainless steel substrate. The intermediate layer serving as a diffusion barrier is required to have the Tamman temperature higher than those of Pd membranes and stainless steel substrates, good

mechanical and thermal stabilities, good adhesion and allowing hydrogen transports [17].

2.4 Diffusion concepts

2.4.1 Diffusion in solids

Diffusion is the phenomenon of material transport by atomic motion. The atoms move from one lattice site to another in a stepwise manner. Two conditions are to be metal: first, an empty adjacent site and second, sufficient energy to break bonds and cause lattice distortions during displacement. If two pieces of different metals are joined together for example, Cu and Ni as in Figure 2.3, which illustrates the schematic atom positions and composition across the interface as the Cu/Ni composite is heated for a long time (but below their melting points). The results indicated that Cu atoms have migrated or diffused into Ni, and that Ni has diffused into Cu [18].
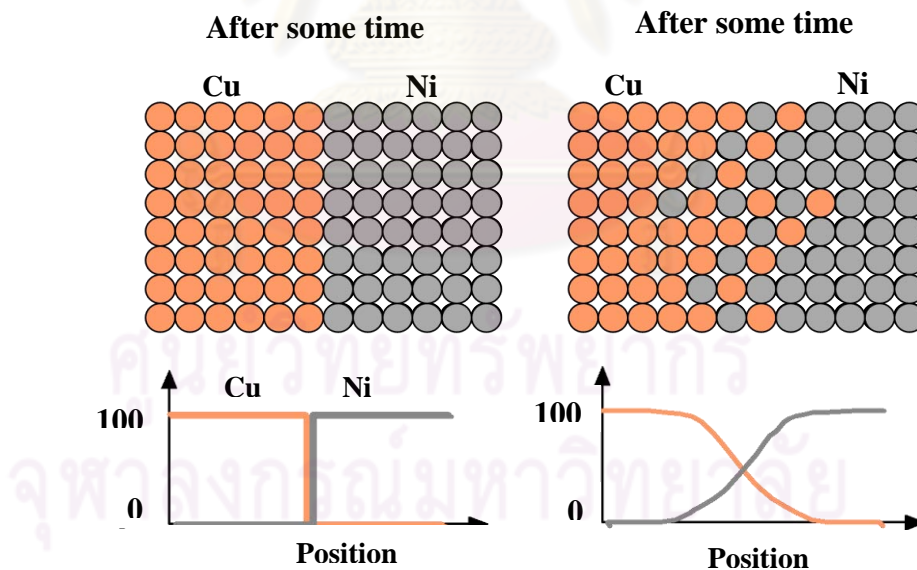
Figure 2.3 Cu-Ni diffusion before and after a high temperature heat treatment.

2.4.2 Mechanisms of diffusion

The first type of diffusions involves the exchange of an atom from its normal lattice position to an adjacent vacant lattice site or vacancy. This is known as "substitutional" or "vacancy diffusion" as shown in Figure 2.4. This process requires the presence of vacancies, and vacancy diffusion depends on the extent of vacancies in the material. The second type of diffusions involves atoms that migrate from an "interstitial" or "in-between" position to a neighboring one that is empty. This occurs with the infusion of impurities such as hydrogen or carbon, which have atoms that are small enough to fit into the interstitial positions as shown in Figure 2.5. Typically, interstitial diffusion is much faster than vacancy diffusion [19].
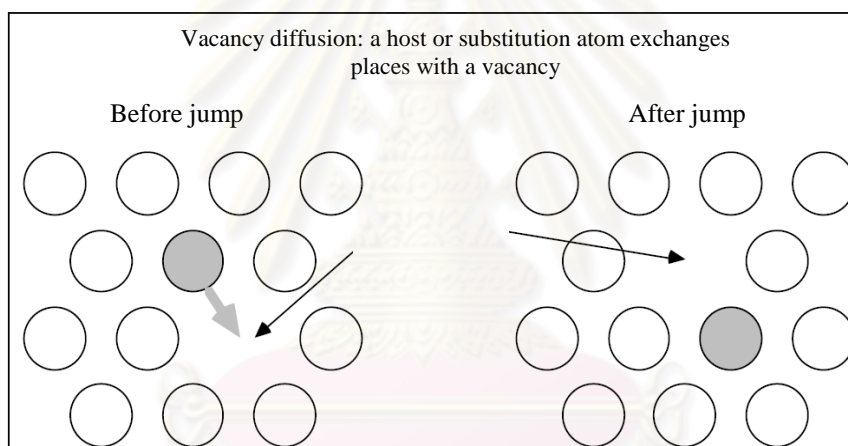
Figure 2.4 Schematic illustration of vacancy diffusion.
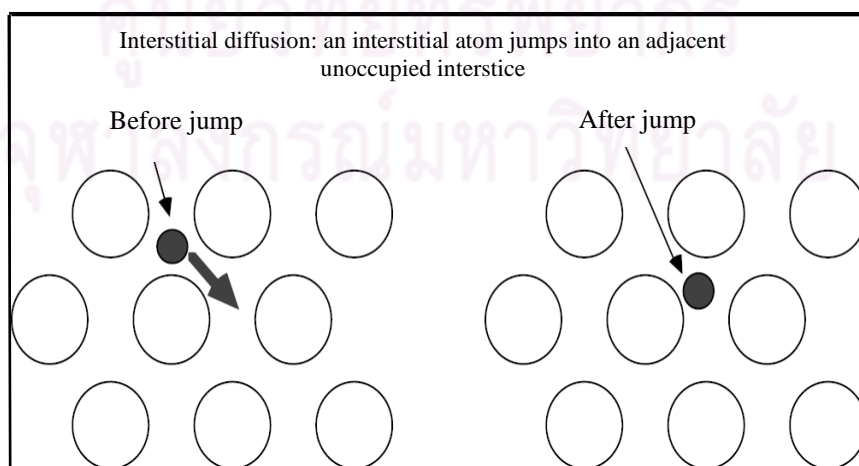
Figure 2.5 Schematic illustration of interstitial diffusion.

2.4.3 Steady-state diffusion

Diffusion is a time-dependent process, and often it is necessary to know how fast it occurs, or the rate of mass transfer. This rate is known as the *diffusion flux*, J, and is defined as the mass, M, diffusing through a unit cross-sectional area of solid, per unit of time. Therefore,

$$ J = \frac{M}{AT} \qquad (2.5) $$

where A is the area across which diffusion is occurring, and T is the elapsed diffusion time. If the diffusion flux does not change with time, a steady state condition exists, and this is called *steady-state diffusion*.
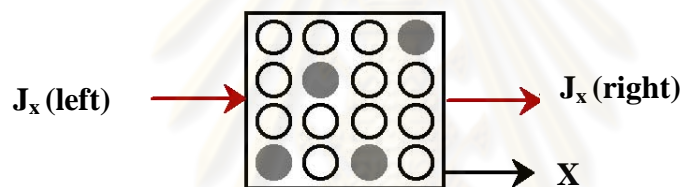
Figure 2.6 Schematic illustration of steady state diffusion [20].

2.4.4 Non-steady state diffusion

Mostly, the diffusion situations are non-steady state. The diffusion flux and concentration gradient varies with time. This is illustrated in Figure 2.7, which shows the concentration profiles at three different diffusion times, the following assumptions are,

- Atoms in the solid are uniformly distributed with the concentration of C_0 before diffusion.
- The value of x at the surface is zero and increases with the distance into the solid.
- Before the diffusion process begins, the time is taken to be zero.
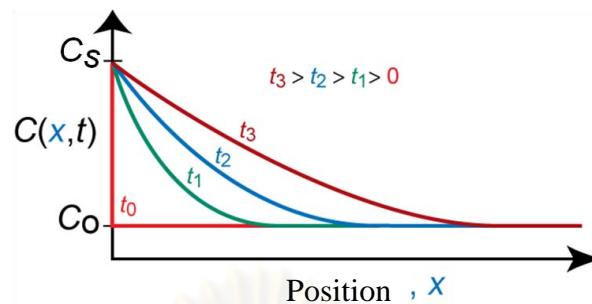
Figure 2.7 Concentration profiles for non-steady state diffusion taken at three different times [21].

2.5 Deposition techniques

There are several plating methods. For example, in one method, a solid surface is covered with a metal sheet, and then heat and pressure are applied to fuse them together (a version of this technique is called Sheffield plate). Other plating techniques include vapor deposition under vacuum, sputter deposition, and methods using vacuum conditions or gas. Recently, however, only plating techniques using a liquid tend to be called "plating". Metallizing refers to the process of coating metal on non-metallic objects [22]. The deposition techniques that used in this work are described in this section.

2.5.1 Electroplating deposition

The process of electroplating is the formation of solid metal on the cathode from ions in a solution, the solution being replenished by metal dissolving from an anode. As the positive ion reaches the cathode, it is neutralized by one or more electrons and the metallic atom so formed either occupies a site on an existing crystal structure or takes part in the nucleation of a new crystal. The amount of metal that is deposited is related to the amount of current [23].

- Electroplating Process

The anode and cathode in the electroplating cell are connected to an external supply of direct current, a battery or, more commonly, a rectifier. The anode is connected to the positive terminal of the supply, and the cathode (an object to be

plated) is connected to the negative terminal. When the external power supply is switched on, the metal at the anode is oxidized from the zero valence state to form cations with a positive charge. These cations associate with the anions in the solution. The cations are reduced at the cathode to deposit in the metallic, zero valence state [24].

Electroplating is the application of electrolytic cells in which a thin layer of metal is deposited onto an electrically conductive surface.
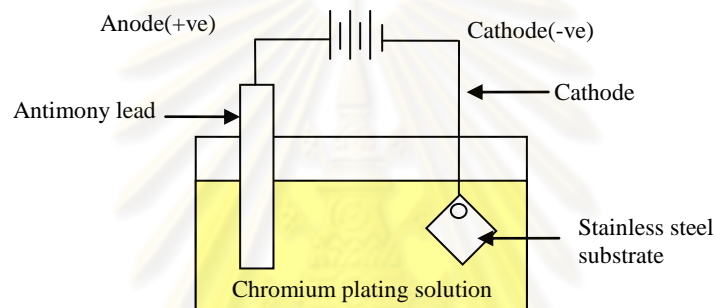
Figure 2.8 Scheme of chromium electroplating

2.5.2 Electroless plating deposition

The deposited of metals on a catalytic surface from solution without an external source of current. This process is used as a preliminary step in preparing plastic articles for conventional electroplating. After cleaning and etching, the surface is immersed in solutions that react to precipitate a catalytic metal *in situ*, Pd, for example. First the substrate is placed in an acidic stannous chloride solution, then into a solution of Pd chloride; Pd is reduced to its catalytic metallic state by the tin. Another way of producing a catalytic surface is to immerse the substrate article in a colloidal solution of Pd followed by immersion in an accelerator solution. The substrate article thus treated can now be plated with nickel or copper by the electroless plating method, which forms a conductive surface which then can be plated with other metals by the conventional electroplating method [26]. Electroless plating, also known as chemical or auto-catalytic plating, is a non-galvanic type of

plating method that involves several simultaneous reactions in an aqueous solution, which occur without the use of external electrical power. Among other techniques, electroless deposition provides strong advantages such as uniformity of deposits even on very complex shapes, very simple equipment and low cost.

Electroless plating is possibly the simplest means of composite membrane fabrication, although substrate quality, surface activation methods, electroless plating procedures and bath chemistry influence membrane selectivity, permeability and Pd/Pd-alloy film stability.

2.6 Phase diagram of alloy

All materials exist in gaseous liquid, or solid form, depending on the conditions of state. State variables include composition, temperature, pressure, magnetic field, electrostatic field, gravitational field, and so on. The term "phase" refers to that region of space occupied by a physically homogeneous material [27]. There are many alloy systems in which a change of temperature causes a change in the relative free energies of the possible phases. The result is that in such cases equilibrium can be maintained during a change of temperature only by the partial or complete replacement of existing phase by new ones. Such rearrangements of the atoms are called phase transformations. In the temperature has been changed too rapidly for equilibrium to be maintained while the temperature is changing. These depend to a large extent on the kinetics of nucleation growth of the new phases [28].

2.6.1 Metal alloying

Alloying, consisting of saturation of surface layers by alloying constituents which are totally or partially soluble in the substrate material, is carried out with power densities greater than those employed in hardening and with longer heating times. By the application of appropriate alloying constituents it is possible to obtain significant enhancement of corrosion resistance. Two types of alloying are distinguished, i.e. remelting and fusion. Remelting, The first type of alloying consists of remelting of coating as well as of the surface layer to a certain depth. The coating may be deposited on the substrate. With the remelting of both layers, their

mixing occurs and the alloying material partially or totally dissolves in the substrate material. After resolidification of the mixture, a different structure and chemical composition to that of the substrate is obtained. The alloying of a solid depends in accordance with the laws of diffusion mainly on the gradient of temperature, gradient of concentration and on time of the diffusion process [29].

2.6.2 Binary Pd-Cu, Pd-Ag and Ag-Cu phase diagram

Annealing and tempering, consisting of heating to a given temperature, soaking at that temperature and cooling at a rate allowing the obtaining of a structure closer to that of equilibrium than the initial structure, are carried out at the lowest possible energy parameters and rather long exposure times. Annealing is used in the technological process of metal strip production in order to homogenize and enhance structure, remove residual stresses and to degas the material [30]. Figures 2.9-2.11 showed the phase diagrams of binary metal alloy which based on our ternary alloy membrane.
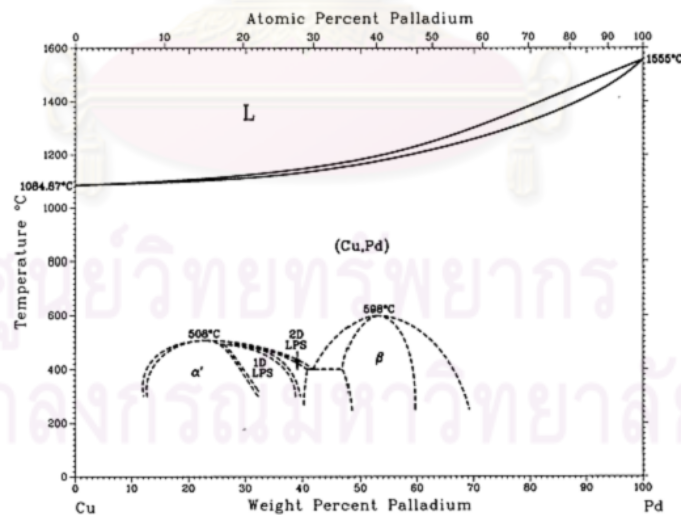
Figure 2.9 Phase diagram of Pd-Cu metal [31].
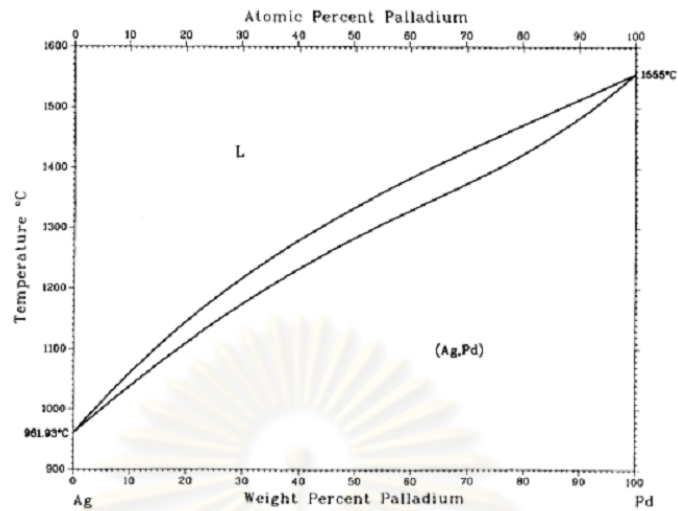
Figure 2.10 Phase diagram of Pd-Ag metal [31].
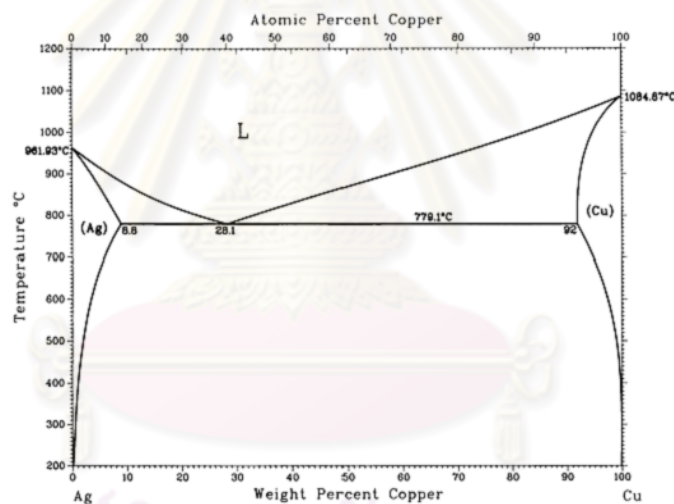
Figure 2.11 Phase diagram of Ag-Cu metal [31].

An alloy is a partial or complete solid solution of one or more elements in a metallic matrix. Complete solid solution alloys give single solid phase microstructure, while partial solutions give two or more phases that may be homogeneous in distribution depending on thermal (heat treatment) history. Alloys usually have different properties from those of the component elements.

2.6.3 Solid solutions

A solution can be defined as a homogeneous mixture in which the atoms or molecules of one substance are dispersed at random into another substance. If this definition is applied to solids, we have a solid solution. The term "solid solution" is used just as "liquid solution" is used because the solute and solvent atoms (applying the term solvent to the element in excess) are arranged at random. The properties and composition of a solid solution are uniform as long as it is not examined at the atomic or molecular level.

Solid solutions in alloy systems may be of two kinds: substitutional and interstitial. A substitutional solid solution results when the solute atoms take up the positions of the solvent metal in the crystal lattice. Solid solubility is governed by the comparative size of the atoms of the two elements, their structure and the difference in electronegativity. When the atomic radii of two elements are equal or differ by less than 15% in size and when they have the same number of valency electrons, substitution of one kind of atom for another may occur with no distortion or negligible distortion of the crystal lattice, resulting in a series of homogeneous solid solutions.

In addition to the atomic size factor, the solid solution is also greatly affected by the electronegativity of elements and by the relative valency factor. The greater the difference between electronegativities, the greater is the tendency to form compounds and the smaller is the solid solubility. Regarding valency effect, a metal of lower valency is more likely to dissolve a metal of higher valency. Solubility usually increases with increasing temperature and decreases with decreasing temperature. This causes precipitation within a homogeneous solid solution phase, resulting in hardening effect of an alloy. When ionic solids are considered, the valency of ions is a very important factor.

An interstitial solid solution results when the solute atoms are small enough to fit into the interstices of the metal lattice. The elements that can form interstitial solid solutions with transition metals are hydrogen, carbon, nitrogen and boron [31].

2.7 Thin films characterization

2.7.1 X-ray diffraction (XRD)

X-ray diffraction (XRD) is a technique used to characterize the crystallographic structure, grain size, preferred orientation in polycrystalline or powdered solid samples, chemical composition, and physical properties of materials and thin films. The diffraction technique is commonly used to identify unknown substances, by comparing diffraction data against a database maintained by the International Centre for Diffraction Data. The X-ray diffraction techniques are based on the elastic scattering of X-rays from structures that have long range order. These techniques are based on observing the scattered intensity of an X-ray beam hitting a sample as a function of incident and scattered angle, polarization, and wavelength or energy [32].

As the crystal lattice is a regular three-dimensional distribution (cubic, rhombic, etc.) of atoms in space. These are arranged so that they form a series of parallel planes separated from one another by a distance d, which varies according to the nature of the material. For any crystal, planes exist in a number of different orientations each with its own specific d-spacing. When a monochromatic X-ray beam with wavelength is projected onto a crystalline material at an angle theta (θ), diffraction occurs only when the distance traveled by the rays reflected from successive planes differs by a complete number n of wavelengths, as illustrated in Figure 2.12. By varying the angle theta (θ), the Bragg's law conditions, are satisfied by different d-spacings in crystalline materials.

$$2d_{hkl}\sin\theta = n\,\lambda \qquad (2.6)$$

λ is wavelength of X- ray beam,

θ is the angle between the incident beam and the scattering planes,

n is an integer.

where n is an integer determined by the order given, λ is the wavelength of the X-rays, d_{hkl} is the spacing between the planes in the atomic lattice, and θ is the

angle between the incident ray and the scattering planes. Plotting the angular positions and intensities of the resultant diffracted peaks of radiation produces a pattern, which is characteristic of the sample. Where a mixture of different phases is present, the resultant diffractogram is formed by addition of the individual patterns [33].

When a monochromatic X-ray beam with wavelength λ is projected onto a crystalline material at an angle theta (θ), diffraction occurs only when the distance traveled by the rays reflected from successive planes differs by a complete number (n) of wavelengths. By varying the angle theta (θ), the Bragg's law conditions, are satisfied by different d-spacing in crystalline material [34].
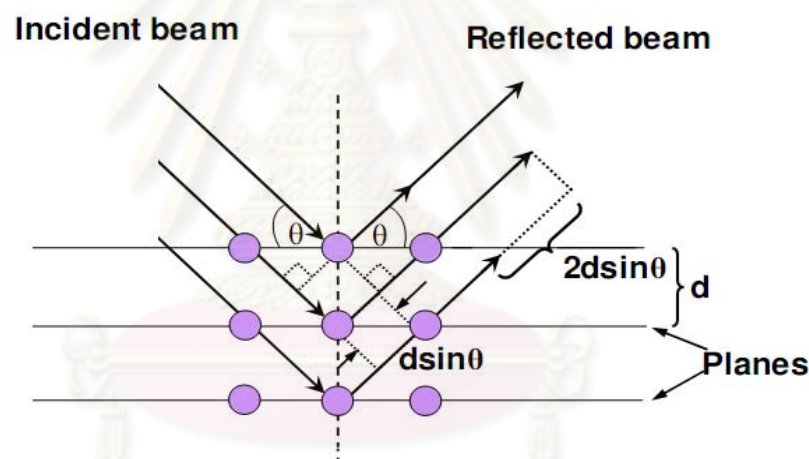
Figure 2.12 Diffraction of X-ray from parallel planes in the crystal followed by Bragg's law.

2.7.2 Scanning electron microscopy with energy dispersive x-ray analysis

Scanning Electron Microscopy (SEM) is a high resolution imaging microscopic technique that uses electrons instead of light to form an image. It has many advantages over traditional microscopes such as a large depth of field, which allows more of a specimen to be in focus at one time, higher resolution, so that closely spaced specimens can be magnified at much higher levels. All of these

advantages, as well as the actual strikingly clear images, make the scanning electron microscope one of the most useful instruments in research today.

For analytical electron microscope, a solid specimen is bombarded in vacuum by a primary electron beam. Once the beam hits the sample and then creates various signals, for example, secondary electrons, backscattered electrons, transmitted electrons, X-rays and Auger electrons, as shown in Figure 2.13. Detectors collect these X-rays, backscattered electrons, and secondary electrons and convert them into a signal that be transformed to the image on the screen.
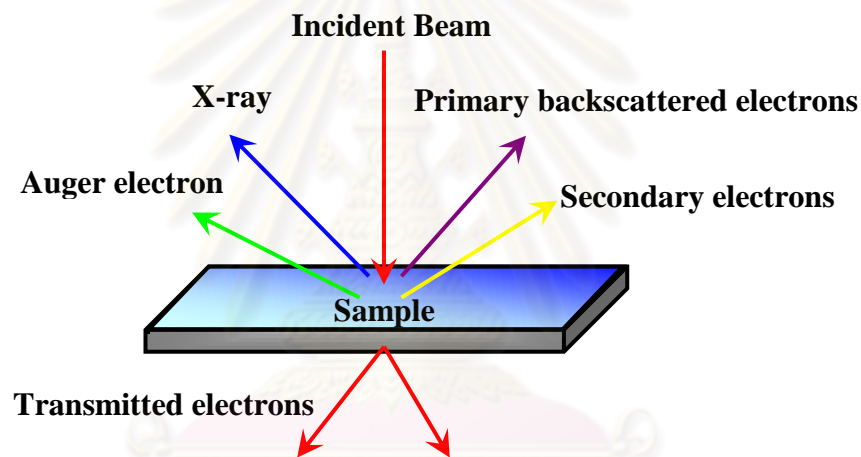
Figure 2.13 Photon and charged particle emission from an electron-bombarded surface [35].

Energy dispersive X-ray analysis (EDS or EDX) is an analytical technique used to determine the composition of the specimens. EDS system works as an integrated feature of the SEM technique which utilizes X-rays that are emitted from the specimen when bombarded by the electron beam.

During EDX analysis, the specimen is bombarded with an electron beam inside the SEM. Those electrons collide with the specimen's own electrons, knocking some of them from the atoms on the specimen's surface. A resulting electron vacancy is filled by an electron from a higher shell. When the electron is displaced, it gives up some of its energy by emitting an X-ray. Each element releases

X-rays with unique amounts of energy during the transfer process, as the finger print of each element. The EDS X-ray detector measures the relative abundance of emitted x-rays versus their energy [36].

2.7.3 Mechanical properties

- **Nanoindentation**

In this work, the CSM™ nanoindentor is used to determine the hardness and elastic modulus of the films. Nanoindentation is mainly consisted of a magnetic loading actuator, a capacitive displacement sensor, a probe, and a sample stage, as shown in Figure 2.14
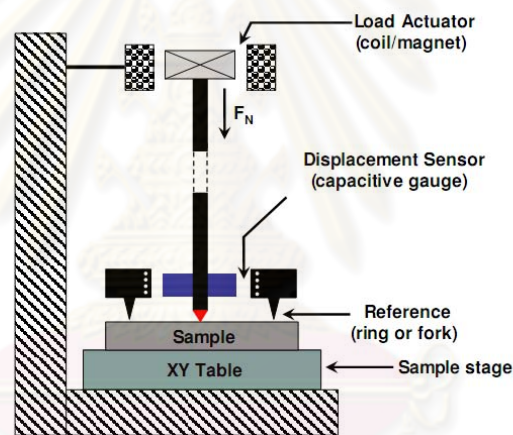
Figure 2.14 Schematic diagram of Nanoindentation [38].

When the indenter is driven into the material, the permanent indent could be happen on the material follow in the geometry indenter tip. The permanent indent is measured for calculate the contact area at maximum load. Thus, the hardness and elastic modulus are obtained by dividing the maximum applied load by the contact area. In the nanoindentation technique, hardness and elastic modulus can be determined by the Oliver and Pharr method, where hardness (H) can be defined as

$$H = \frac{P_{max}}{A} \, ,$$

where P_{max} is the maximum applied load,

          A   is the contact area at maximum applied load.

The typical load-displacement curve, showing the values used in the Oliver and Pharr method [37], as showed in Figure 2.15
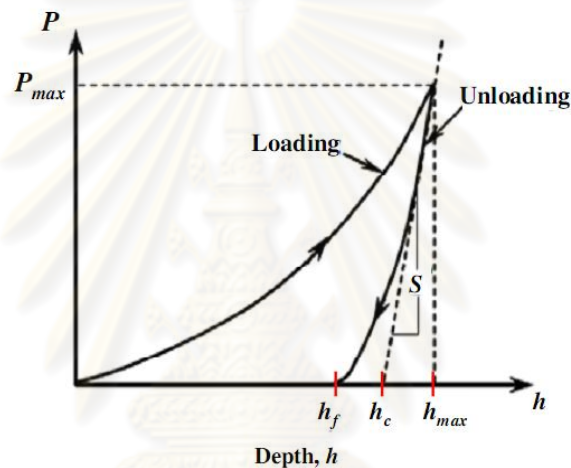
Figure 2.15 Schematic diagram of the typical load-displacement curve [38].

Where h_f is the final unloading depth,

          h_{max} is the maximum indentation depth at maximum applied load,

          P_{max} is the maximum applied load,

          h_c is the contact depth.

2.8 Literature survey

In 2009, Peters *et al.* [39] investigated the hydrogen permeation and stability of tubular Pd alloy (Pd-23w%Ag) composite membranes have been investigated at elevated pressures. A maximum hydrogen flux of 1223 was obtained at 40°C and 26 bar hydrogen feed pressure, corresponding to a permeance of 6.4×10^{-3} mol·m^{-2}·s^{-1}·Pa$^{-0.5}$. A good linear relationship was found between the square root of the have been investigated at elevated pressures. A maximum H$_2$ flux of 1223

was obtained at 40°C and 26 bar hydrogen feed pressure, corresponding to a permeance of 6.4×10^{-3} mol·m^{-2}·s^{-1}·Pa$^{-0.5}$. A good linear relationship was found between the square root of the hydrogen flux and pressure as predicted for rate controlling bulk diffusion. In a mixture of 50% H_2+50% N_2 a maximum H_2 flux of 230 mL·cm^{-2}·min^{-1} and separation factor of 1400 were achieved at 26 bar.

In 2005, Lin *et al*. [40] studied electroless plating synthesis of Pd-Cu alloy films on PSS substrate modified with Pd seeded ZrO_2 layer. This intermediate layer served as an intermetallic diffusion barrier that improved the membrane stability. For electroless plating process, they found that the excessive amount of hydrazine hydrate resulted in precipitation of a great deal of Pd powders in the plating bath. To prevent this phenomenon, several divided hydrazine hydrate batches was added into the plating bath during electroless plating. $Pd_{46}Cu_{54}/ZrO_2$ PSS composite membranes were found to exhibit no nitrogen permeation flux with H_2 permeation of 1.1×10^{-7} molm^{-2}s^{-1} Pa at 753 K.

In 2005, Lee *et al*. [41] fabricated pinhole-free Pd/Ni alloy composite membrane with a diffusion barrier on porous stainless steel substrates by vacuum electrodeposition. To improve the structural stability of Pd alloy/Ni 316L stainless steel composite membrane, they prepared a thin intermediate layer of TiN by a sputtering method. The TiN thin film was introduced as a diffusion barrier between the Pd/Ni layer and stainless steel substrate. The results suggested that the Pd/Ni layer and alloy composite membrane with a diffusion barrier of TiN yielded a high separation performance for hydrogen and showed very good stability under the mixture gas of 50% H_2 and 50% N_2 for an operation time of more than 60 days.

In 2006, Ryi *et al*. [6] fabricated of Pd-Cu-Ni alloy membrane deposited 4 min thickness on porous nickel substrate by multi target sputtering and Cu-reflow technique. The surface of porous nickel substrate needed not to be modified because it has very uniform and small pore distribution as 33 nm. From the XRD and SEM analysis, it was clarified that the fabricated Pd-Cu-Ni ternary alloy film had Pd-Cu-Ni alloy character and no defects on the surface of thin membrane. The weight composition of Pd:Cu:Ni was 89:4.5:6.5 from EDS analysis. Furthermore, hydrogen separation factor with single gas test was infinity indicating pinhole-free Pd-based

alloy membrane. In addition, it was so stable that the morphology of the surface was not changed and there were no indications of metal interdiffusion during time-on-stream test for 10 days with the cycling of operating temperature and transmembrane pressure difference. Furthermore, there were no indications of the metallic interdiffusion between Pd-Cu-Ni alloyed membrane and nickel substrate from the membrane analysis after stability test.

In 2007, Wang *et al*. [42] studied the Pd-Ag-Ru/γ-Al$_2$O$_3$ ternary alloy composite membrane is fabricated by simultaneous electroless plating of Pd, Ag and Ru on to the outside surface of porous γ-Al$_2$O$_3$ substrate, followed by annealing. The composition of fabricated dense Pd-Ag-Ru/γ-Al$_2$O$_3$ ternary alloy composite membrane has been identified as Pd$_{69}$Ag$_{30}$Ru$_1$/γ-Al$_2$O$_3$ by ICP-AES analysis. The traditional Pd-Ag/γ-Al$_2$O$_3$ binary alloy composite membrane and Pd/γ-Al$_2$O$_3$ composite membrane are also fabricated for their comparison with Pd-Ag-Ru/γ-Al$_2$O$_3$ membrane. The ternary alloy composite membrane of Pd$_{69}$Ag$_{30}$Ru$_1$/γ-Al$_2$O$_3$ exhibits unique high hydrogen permeability in comparison with Pd/γ-Al$_2$O$_3$ membrane or with Pd-Ag/γ-Al$_2$O$_3$ binary alloy membrane. The permeability of Pd$_{69}$Ag$_{30}$Ru$_1$/γ-Al$_2$O$_3$ membrane is about three to four times higher than that of γ-Al$_2$O$_3$ membrane.

In 2006, Ayturk *et al.* [43] prepared the intermetallic diffusion barrier layer by the controlled in-situ oxidation method for Pd and Pd/alloy porous stainless steel composite membrane was investigated. SEM and EDS results showed the existence of an oxide layer as the intermetallic diffusion barrier for oxidation temperatures higher than 600°C. At oxidation temperatures lower than 600°C, there might still be an oxide layer at the membrane substrate interface although it was too thin to be detected by SEM and EDS. The alloy formation study showed that annealing at 500°C under helium atmosphere did not produce alloys with uniform compositions either for Pd/Ag or Pd/Cu membranes. However, annealing at 600°C gave a uniform Pd/Cu porous stainless steel (PSS) composite membrane, with no detectable presence of elements from the PSS substrate, further demonstrating the oxide layer as an effective intermetallic diffusion barrier.

In 2000 Stefanov *et al*. [44] prepared the chromium oxide films formed on stainless steel by immersion in a chromium electrolyte and studied the structure and composition by SEM and XPS. Cr_2O_3 crystallites in the range 30-150 nm are fully developed and covered the whole surface. The chemical compositions in the depth and the thickness of the oxide layer have been determined by XPS sputter profiles. The oxide film can be described within the framework of a double layer consisting of a thin outer hydrated layer and an inner layer of Cr_2O_3.

CHAPTER III

EXPERIMENTAL

3.1 Experimental details

The experiment was divided into 4 main parts:

3.1.1 Preparation of non-porous and porous 316L stainless steel substrate

3.1.2 Preparation of binary Pd-Cu, Pd-Ag and ternary Pd-Ag-Cu alloy membranes

3.1.3 Membrane characterizations

3.1.4 Hydrogen permeation flux testing

3.1.1 Preparation of non-porous and porous 316L stainless steel substrates

100-cm^2 sheets of stainless steel were cut into 1-cm^2 specimen and drilled at one corner. The general procedure for cleaning the substrate was showed in Figure 3.1.

Alkaline solution   DI water   Iso-propanol
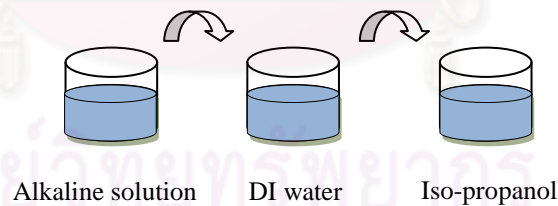
Figure 3.1 Step for cleaning of the substrates.

➢ **Surface cleaning with an alkaline solution**

The substrates were cleaned in an ultrasonic bath at ~60°C for one hour and then washed thoroughly three times with de-ionized (D.I.) water. Finally, the substrate was cleaned again by iso-propanol to remove any trace amount of water and dried at 120°C for 3 hours. The chemical composition of the alkaline solution is given in Table 3.1.

Table 3.1 Composition of the alkaline solution for cleaning the substrates.

Compound	Concentration
Sodium phosphate, $Na_3PO_4 \cdot 12H_2O$	45 g/L
Sodium carbonate, Na_2CO_3	65 g/L
Sodium hydroxide, NaOH	45 g/L
Detergent	4 ml/L

3.1.2 Preparation of binary Pd-Cu, Pd-Ag and ternary Pd-Ag-Cu membranes

3.1.2.1 Preparation of binary Pd-Cu membranes

3.1.2.1.1 Electroless plating of Pd membranes

Prior to electroless plating process of Pd layer, the surface of the substrate was activated to seed palladium nuclei, initiating the autocatalytic process during Pd electroless plating. After complete the Pd layer then, the Cu layer was deposited on top of Pd by electroplating method for 1-5 min, depend on composition of the alloy. After that the layers were annealed in argon atmosphere at 750°C for 20 hours, as shown in a flowchart in Figure 3.2 [43].
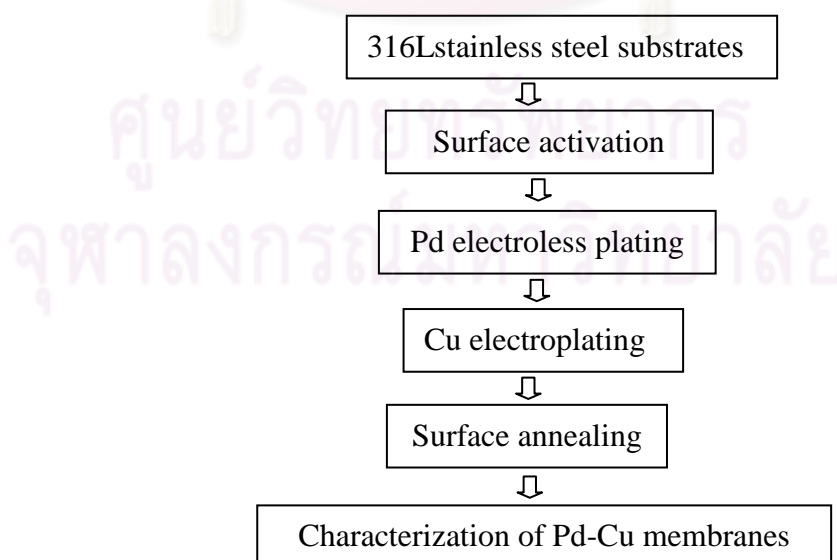
Figure 3.2 Schematic of general procedure for Pd-Cu membranes.

For more details, the surface activation solutions for Pd, including tin chloride ($SnCl_2$) solution, palladium chloride ($PdCl_2$) solution and hydrochloric solution 0.01 M (HCl) were prepared as follow:

- Preparation of $SnCl_2$ solution

In to 1.0 L volumetric flask, we added approximately 200 mL DI water, 1.0 mL of 10 M (concentrated, ~37%) HCl and 1.0 g of $SnCl_2.H_2O$, then shake gently to dissolve. After that, more DI water was filled to make up to 1.0 L.

- Preparation of $PdCl_2$ solution

In to 1.0 L volumetric flask, we added approximately 200 mL DI water, 1.0 mL of 10 M (concentrated, ~37%) HCl, 0.1 g $PdCl_2$ and heat up to ~60°C with stirring until dissolved (usually for approximately half an hour). Then, make up to 1.0 L by filling with DI water.

- Preparation of 0.01 M HCl solution

In to 250 mL volumetric flask, we added approximately 250 mL DI water, 1.0 mL of 10 M (concentrated, ~37%) HCl and make up to 1.0 L with DI water.

In surface activation process, the substrates were immersed in $SnCl_2$ solution, DI water and $PdCl_2$ solution. Then, the substrates were rinsed with 0.01 M of $SnCl_2$ to remove any trace amount of tin compounds on the surface and finally, rinsed with DI water. This cycle, as shown in Figure 3.3 was repeated at least six times. After activation, the surface activated substrates were dried at 120°C for 3 hours. A perfectly activated surface has a smooth and dark-brown in color.
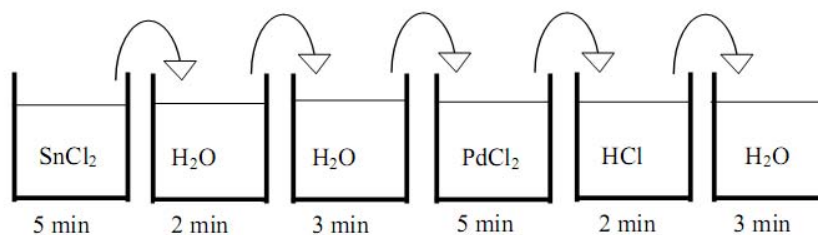
Figure 3.3 One loop of the activation process.

In this traditional activation process, the substrates were dipped in acidic solutions of Sn^{+2} and Pd^{+2} salts respectively with gentle rinsing in de-ionized water between two baths. Sn^{+2} is absorbed on the substrate surface in hydrolytic form (sensitization step) and replaced by Pd^0 through the process. This repeating is to produce enough Pd particles for further deposition of Pd as shown in Equation (3.1) [44].

$$Sn^{+2} + Pd^{+2} \rightarrow Sn^{+4} + Pd^0 \tag{3.1}$$

Table 3.2 Chemical composition of electroless Pd plating solution.

Compound	Concentration
Tetraaminepalladium (II) chloride, $Pd(NH_3)_4Cl_2 \cdot H_2O$	4.0 g/L
Ammonia solution, NH_4OH (28%)	198 mg/L
Disodium ethylenediamminetetraacetate, Na_2EDTA	40.1 g/L
Hydrazine hydrate, $N_2H_4 \cdot H_2O$	5.6 - 7.6 ml/L

Electroless plating is a combination of the cathodic deposition of metal and the anodic oxidation of reductant at the immersion potential. Pd deposition occurs as the result of the following simultaneous reactions:

Figure 3.4 Pd plating bath.

Anodic Reaction:

$$N_2H_4 + 4OH^- \rightarrow N_2 + 4H_2O + 4e^- \tag{3.2}$$
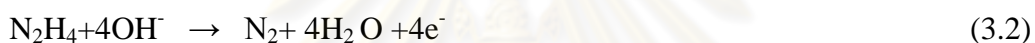
Cathodic Reaction:

$$2Pd[NH_3]_4^{2+} + 4e^- \rightarrow 2Pd^0 + 8NH_3 \tag{3.3}$$
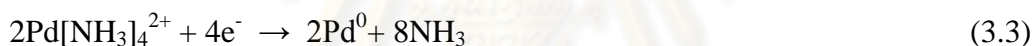
Autocatalytic Reaction:

$$2Pd[NH3]_4^{2+} + N_2H_4 + 4OH^- \rightarrow 2Pd^0 + N_2 + 4H_2O + 8NH_3 \tag{3.4}$$
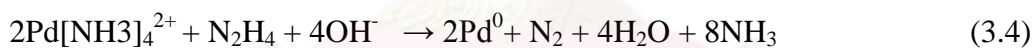
The reaction occurs on the surface of the activated substrate, and preferentially around the Pd seeds. It is initiated by the reaction of hydrazine with hydroxide ions forming nitrogen gas and water with simultaneous release of electrons. The electrons are transferred across the Pd island and used for the decomposition of Pd-amine complex into Pd metal and ammonia gas. The Pd metal is deposited onto the nuclei resulting in growth. The deposition rate increase with the number of Pd sites and exhibits autocatalytic behavior. Nitrogen and ammonia gases are evolved as bubbles during the plating process.

3.1.2.1.2 Electroplating of Cu membranes

Electroplating is the application of a metal coating to a metallic or other conducting surface by an electrochemical process. The object to be plated is used as the cathode (negative electrode) of an electrolysis cell through which a direct electric current is passesd. The object is then immersed in an aqueous solution containing the required metal in an oxidized form, either as an aquated cation or as a complex ion. The anode is usually a bar of the metal being plated, in this case copper. During electrolysis metal is deposited on to the work and metal from the bar dissolves:

at cathode: $CuSO_4(aq) + 2e^- \rightarrow Cu(s)$ (3.5)

at anode: $Cu(s) \rightarrow Cu^{2+}(aq) + 2e^-$ (3.6)
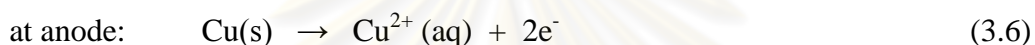
- Preparation of $CuSO_4$ solution

$CuSO_4$ solution was prepared by using DI water to dissolve 25.0 g $CuSO_4$ in 100 ml volumetric flask. The plating condition for Cu was done at room temperature and 2.0 V potential was used for plating the Cu layer as shown in Figure 3.5.

Power supply

Cu wire

Substrate for plating
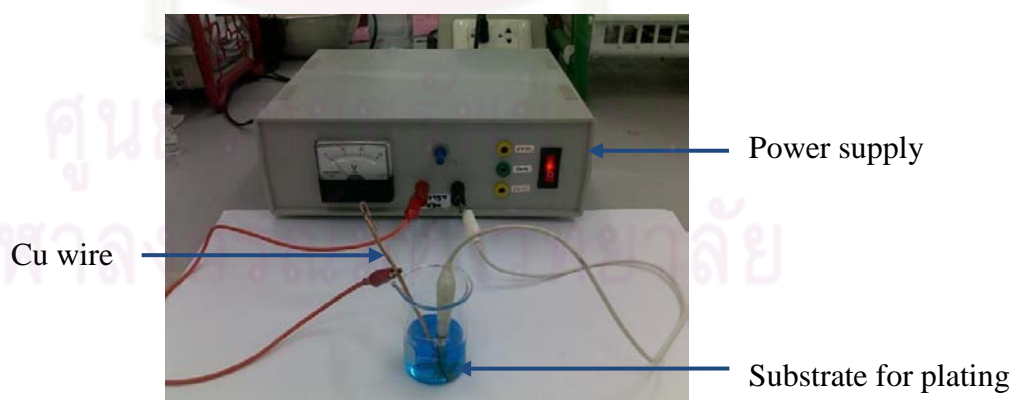
Figure 3.5 Schematic of Cu electroplating.

- **Alloy annealing[43]**

After the plating the Pd-Cu membranes, the samples were annealed at 750°C in argon atmosphere for 12 hours to promote alloying.

3.1.2.2 Preparation of binary Pd-Ag membranes

The Pd-Ag layers were made following the flowchart in Figure 3.6. The Pd-Ag alloy membranes had a fixed thickness of plated Pd at 200 nm (deposition time of 180 min) and the plating time for Ag was varied from 1-5 seconds. After both layers were done, the annealing in argon atmosphere at 900°C for 20 hours was taken place [45].
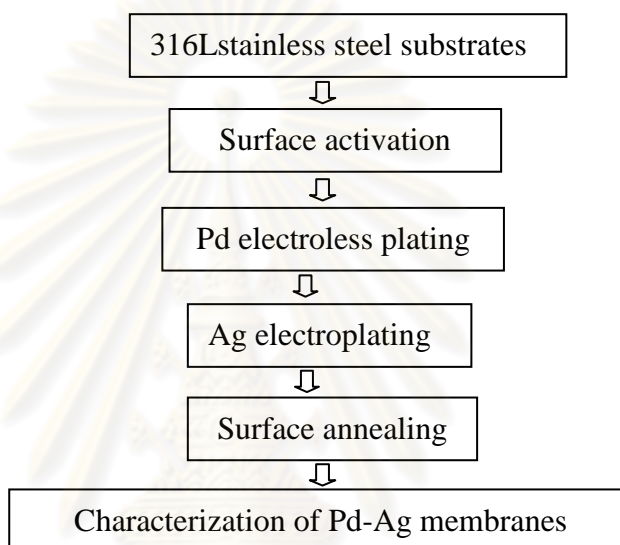
Figure 3.6 Schematic of general procedure for plating Pd-Ag membranes.

3.1.2.2.1 Electroless plating of Pd membranes

After the cleaning and surface activation, electroless plating of Pd membrane was electroless-plated on the substrates, as the procedure described in the last section, at a fixed deposition time of 180 minutes.

3.1.2.2.2 Electroplating of Ag membranes

- Preparation of AgNO$_3$ solution

AgNO$_3$ solution was prepared by using DI water to dissolve 10.0 g AgNO$_3$ in 100 ml volumetric flask. The plating condition for Ag was done at room temperature and 1.0 V potential was used for plating the Ag layer as shown in Figure 3.7.

The plating baths were kept at the room temperature during electroplating. Prior to Ag electroplating, the seed surface was pretreated with sulfuric acid. Then, area was exposed to the plating electrolyte. 99.9% pure Ag wire was used as a counter electrode shown in Figure 3.7.

Power supply

Ag metal

Substrate for plating
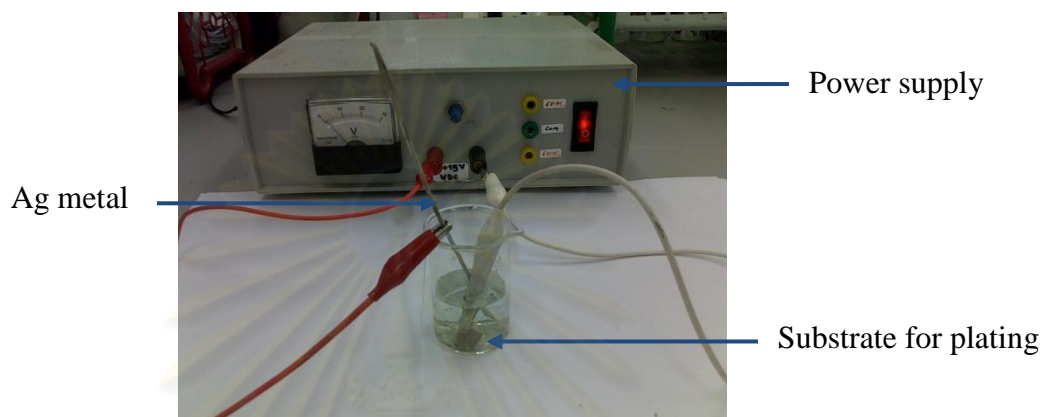
Figure 3.7 Schematic of Ag electroplating.

at cathode $AgNO_3(aq) + e^- \rightarrow Ag(s)$ (3.7)

at anode $Ag(s) \rightarrow Ag^+(aq) + e^-$ (3.8)
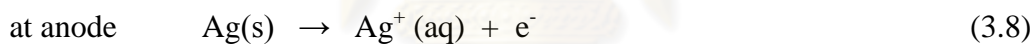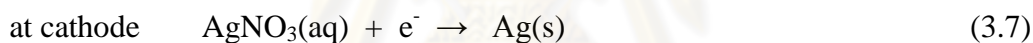
3.1.2.3 Preparation of ternary Pd-Ag-Cu membranes

For ternary membranes of Pd-Ag-Cu in this study shown in Figure 3.8, the Pd, Ag and Cu were deposited on the 316L stainless steel as follow:

3.1.2.3.1 Electroless plating of Pd membranes

Before Pd plating, the substrates surface was activated with $SnCl_2$ and $PdCl_2$ and the Pd membrane was deposited at 60°C by electroless plating for 180 minutes.

3.1.2.3.2 Electroplating of Ag membranes

For Ag electroplating, $AgNO_3$ 100 g/L was electrolysed for 3 seconds.

3.1.2.3.3 Electroplating of Cu membranes

For Cu electroplating, $CuSO_4$ 250 g/L was electrolysed deposited on the top of Pd-Ag membrane for 1-3 minutes.

```
┌─────────────────────────────────────┐
│   316L stainless steel substrates    │
└─────────────────────────────────────┘
                  ⇩
        ┌─────────────────────┐
        │  Surface activation │
        └─────────────────────┘
                  ⇩
        ┌─────────────────────┐
        │ Pd electroless plating │
        └─────────────────────┘
                  ⇩
        ┌─────────────────────┐
        │   Ag electroplating │
        └─────────────────────┘
                  ⇩
        ┌─────────────────────┐
        │   Cu electroplating │
        └─────────────────────┘
                  ⇩
        ┌─────────────────────┐
        │   Surface annealing │
        └─────────────────────┘
                  ⇩
┌─────────────────────────────────────┐
│  Characterization of Pd-Ag-Cu membrane │
└─────────────────────────────────────┘
```
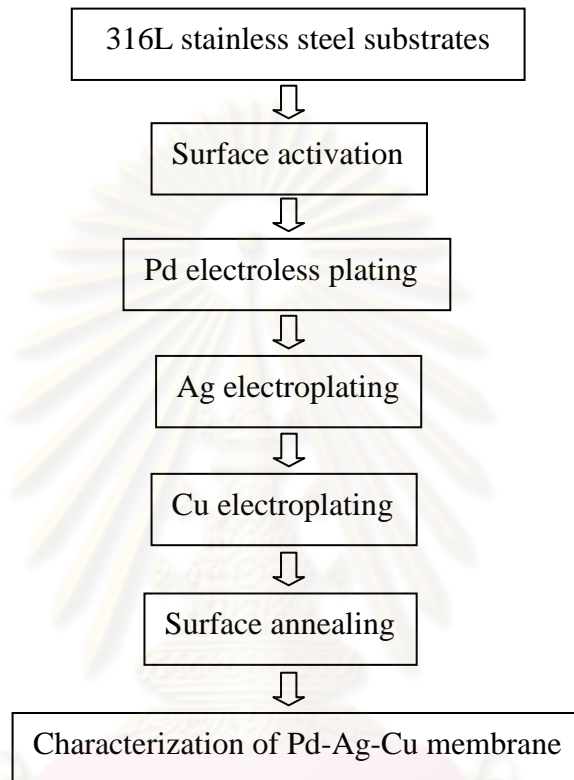
Figure 3.8 Schematic of general procedure for Pd-Ag-Cu membranes.

o **Preparations of Cr_2O_3 intermetallic diffusion barriers**

Electroplating followed by thermal oxidation were employed in preparing the diffusion barrier

➤ **Electroplating/oxidation**

The electroplating device setting is depicted in Figure 3.9. The chromium plating solution consisted of 250 g/L chromic acid and 1.25 g/L sulfuric acid as a catalyst in 200:1 ratio. The chromium plating was performed at room temperature with current density ~100-150 A/ft^2.
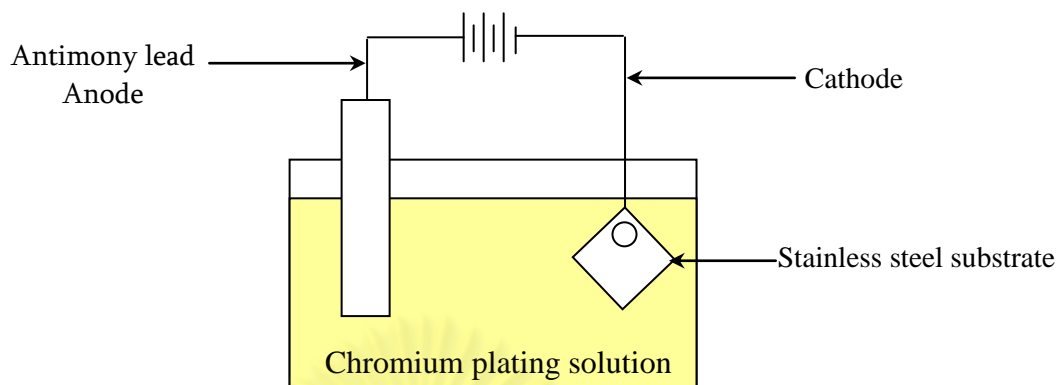
Figure 3.9 The chromium electroplating device.

Then the chromium oxide layer was generated by oxidizing in air at 600°C and oxidation times 6 hours [36].

- **Alloy annealing**

The Pd-Ag-Cu metal films were deposited on 316L stainless steel substrates. And then were annealed in an argon flow at 1100°C during 20 hours.

3.1.3 Membrane characterizations

- **SEM and SEM-EDX**

The membranes were evaluated by using a scanning electron microscope (SEM), equipped with an energy dispersive X-ray analysis (EDS) to measure the thickness of the coated film and determine the elemental compositions of the plated alloy membrane.

- **X-ray diffractrometer (XRD)**

The physicale structures of membrane layers were examined by an X-ray diffractometer (XRD) in 2θ-mode to identify the crystal structure and preferred orientation of the crystal plane, as well as the alloy formation.

Figure 3.10 X-ray diffractrometer (XRD), Rigaku Geigerflex X-ray diffractometer equipped with a CuK-radiation source**.**

- **Mechanical characterization by nanoindentation**

The mechanical properties of the films were measured by nanoindentation system (CSM instrument), which illustrated in Figure 3.11. A Berkovich three-sided pyramid indenter tip was used in this study. Before measurement, calibration was performed on the fused silica (FS) standard, which is normally used to calibrate due to its low modulus to hardness ratio [46]. Then, the experiment was carried out and calculated from load-unload curve by using the Oliver-Pharr calculation method.
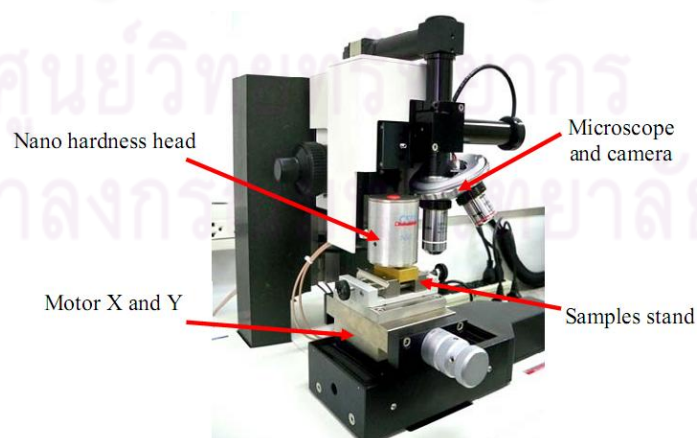
Figure 3.11 The nanoindentation tester (CSM instruments) at Center for Innovative Nanotechnology, Chulalongkorn University.

3.1.4 Hydrogen permeation flux testing

In experimental for hydrogen permeation flux testing, the alloy membranes have been deposited on the disk-shaped 316L porous stainless steel substrate with a thickness of 1 mm and an average pore size of 0.2 μm. Permeation experiments were carried out using pure hydrogen in a conventional gas permeation apparatus. The alloy membrane was loaded into a stainless steel shell and centered in a tube furnace. For membrane sealing, graphite ring gaskets were used. The membranes were subjected to helium flux measurement until no more helium flux was detected from the outlet of the permeation cell, indicating that Pd, Pd-Cu, Pd-Ag and Pd-Ag-Cu membranes were dense and covered completely on the PSS area. The permeation for all runs was done under atmospheric pressure. The dense Pd membrane disk was heated in helium at a rate of about 4°C/min before subjecting to hydrogen at 350°C. Dense Pd membranes should not allow helium permeation through the permeation cell, shown in Figure 3.12. The pressure of the feed gas was monitored at 1-3 atm and the temperature of the reactor was varied from 350 to 500°C. The gas permeation rate was measured by a soap-bubble flow meter. The diagram of apparatus set up for hydrogen permeation flux testing was shown in Figure 3.13.
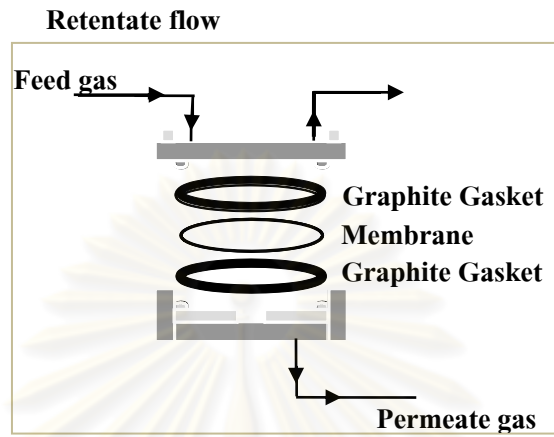
Figure 3.12 The permeation cell.
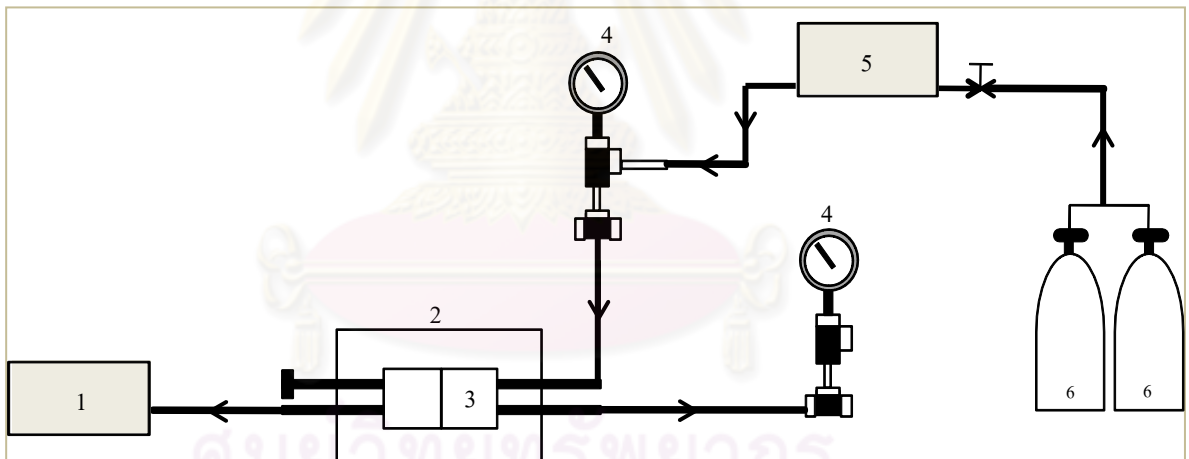
Figure 3.13 The hydrogen gas permeation set up.

1. Digital flow meter   2. Furnace   3. Permeation cell

4. Pressure gauge   5.Gas controller   6. Gas cylinder

CHAPTER IV

RESULTS AND DISCUSSION

Thin Pd-alloy membrane was fabricated by electroless and electroplating depositions of metals onto 316L stainless steel substrates. Three elements of metal, Pd-Ag-Cu membranes were fabricated and tested for hydrogen separation in various working temperatures. The metallic alloy membranes were characterized by using SEM, SEM/EDS and XRD analysis. It has already been realized that the advantage of non-porous Pd-alloy membrane over porous stainless steel substrates have high selectivity and hydrogen permeance. In this study, Pd was a selected material as a based material for developing as a dense Pd-alloy membrane which can lead to a higher hydrogen permeation, improve the mechanical properties, low cost, resistance to embrittlement, thermal stability and also increases resistance to chemical contaminants [47].

4.1 Preparation of 316L stainless steel substrates

Non-porous and porous 316L stainless steels were chosen as a substrate because it has high resistance to corrosion. It is also tougher and stronger than other materials, for example, ceramic and glass that used as substrates in other works [48]. In addition, it is suitable for the process of electroless plating and electroplating technique which were used for developing the thin film of Pd-Ag-Cu membrane, following Mardilovich et al. [49].

Figure 4.1 shows the SEM micrographs, indicating the surface image of non-porous stainless steel and porous stainless steel substrates. The pore size distribution of porous stainless steel substrate, is much larger than pores that could be observed on the surface of the normal stainless steel.
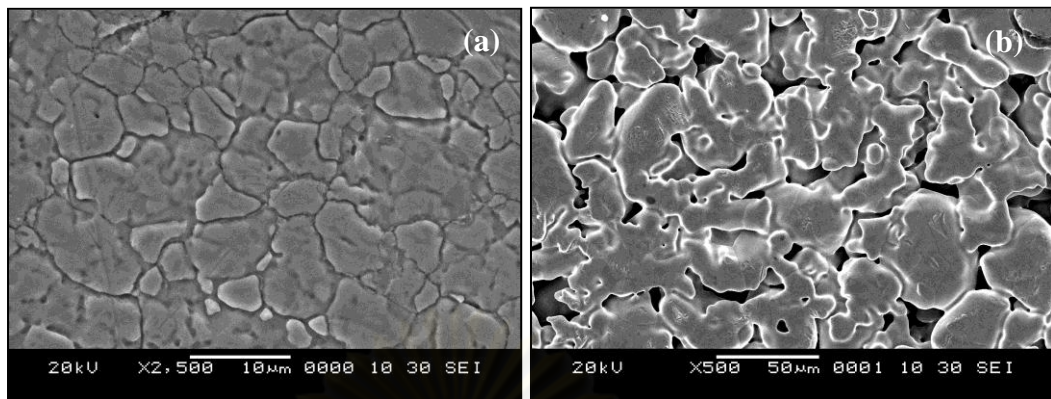
Figure 4.1 SEM images of (a) stainless steel (SS) substrate and (b) porous stainless steel (PSS) substrate.

4.2 Deposition rate of Pd, Cu and Ag in plating process

   In this study, deposition rate of Pd, Cu and Ag was investigated. This shows the layer thickness was increased as the deposition time increased. In addition, the deposition rate of Pd membrane has 6.80 nm/minute by using electroless plating techniques.
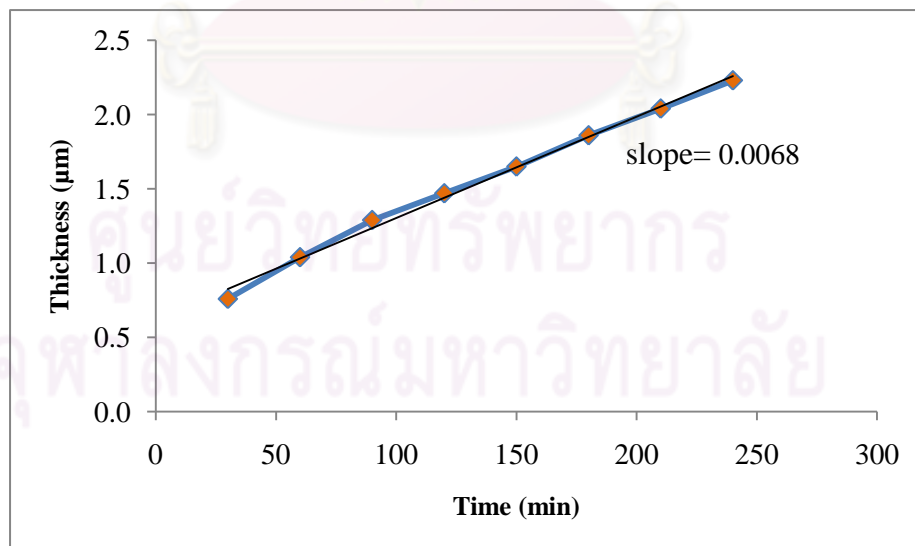
Figure 4.2 Deposition rate of Pd by electroless plating.

   The deposition rate of Cu and Ag layers, fabricated by electroplating techniques, was 0.1054 µm/minute and 16.68 µm/minute, respectively.
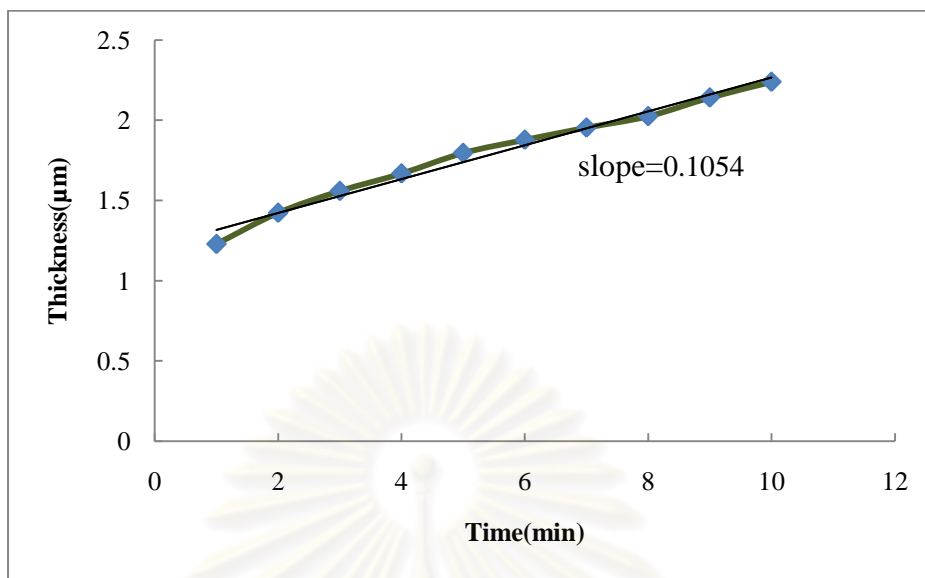
Figure 4.3 Deposition rate of Cu electroplating.
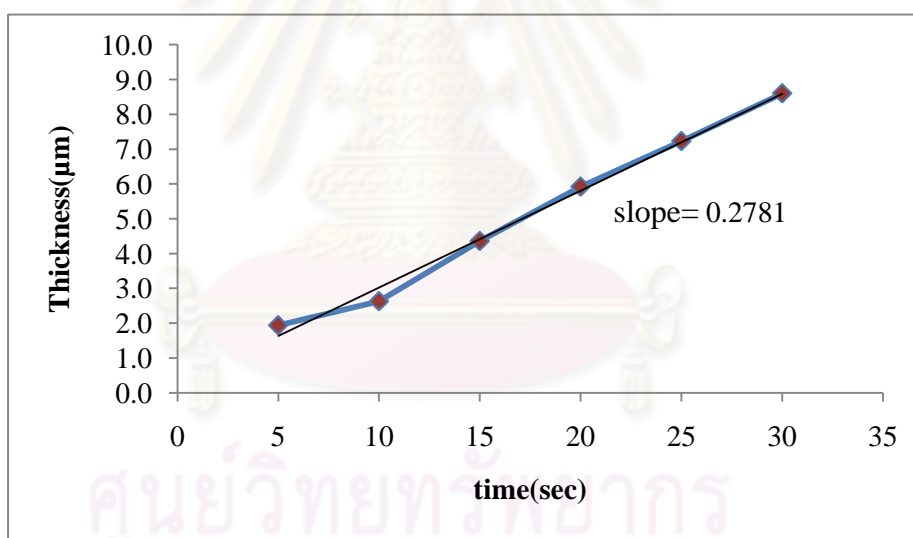
Figure 4.4 Deposition rate of Ag electroplating.

Thin Pd film membrane was conducted by electroless plating. Ag and Cu were deposited by electroplating on the 316L stainless steel substrates. The membranes were controlled by deposition time and condition for plating. The Pd, Ag and Cu layer showed a good adhesion and successfully deposited on the substrate. The thickness and time of deposition were plotted, as shown in Figures 4.2-4.4, and rate for plating was calculated from the slope of graph.

The electroless and electroplating techniques have several advantages over other techniques, particularly on the operational flexibility, simplicity of equipment, cost performance and uniformity of metal deposition on the substrates. The electroplating technique can produce a high quality to metal deposition because it made with the current source and easy to controlling the deposition. On the other hands, the electroless plating technique can also produce a high quality to metal deposition, however it has some difficulties to control the reactions and use a longer deposition time, compared to electroplating technique.

4.3 Preparation of Pd-Cu, Pd-Ag and Pd-Ag-Cu alloy membrane

The electroless plating and electroplating technique were used in the preparation of the thin film of Pd-alloy membrane. The procedure is composed of steps:

(1) Surface cleaning of the substrate for degreasing

(2) Surface activation with $SnCl_2$ and $PdCl_2$ for reducing the plating time

(3) Pd plating with $Pd(NH_3)_4Cl_2$ solution

(4) Ag plating with $AgNO_3$ solution

(5) Cu plating with $CuSO_4$ solution

(6) Surface annealing in argon atmosphere

The details of each step are described as follows:

➤ **Surface cleaning**

The 316L stainless steel of 1x1 cm^2 sheets were cleaned with either an alkali solution or commercial solvents. This process is very important due to the Pd plating could not be deposited successfully because of grease, oil, dirt, corrosion products and others existing on the stainless steel surface.

➢ **Surface activation**

The next step was the activation of the stainless steel surface, in order to initiate an autocatalytic process of the reduction of a metastable salt complex on the target surface during electroless plating. This was performed by the repeated, alternate treatments with $SnCl_2$ and $PdCl_2$ solutions. The SEM image of the 316L stainless steel surface before and after surface activation was showed in Figure 4.5. It clearly indicated that the surface was effectively activated. A large number of seeds with relatively uniform particles on the substrate surface were observed.
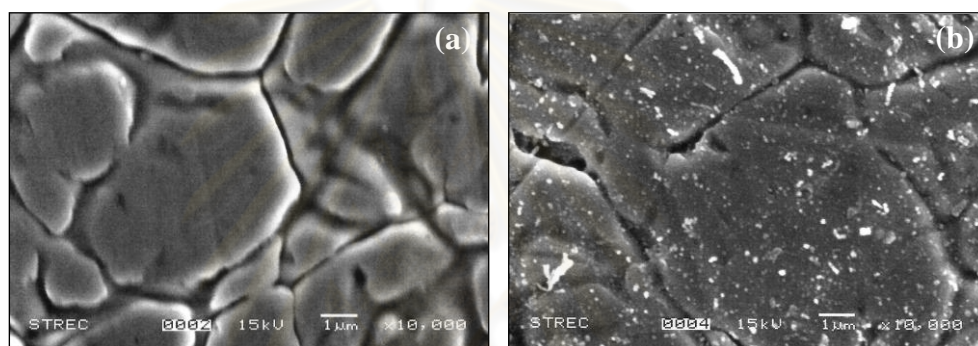
Figure 4.5 SEM images of (a) the stainless steel before surface activation and (b) after surface activation.

$$2SnCl_2 + 3H_2O \longrightarrow 2Sn(OH)_{1.5}Cl_{0.5} + 3HCl \qquad (4.1)$$
$$Pd^{2+} + Sn^{2+} \longrightarrow Pd^0 + Sn^{4+} \qquad (4.2)$$
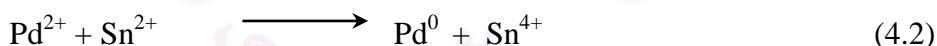
It was found that tin nuclei were created by decomposing $SnCl_2$ to $Sn(OH)_{1.5}Cl_{0.5}$ with deionized water according to equation 4.1, followed by the deposition of Pd on the tin layer via the redox process as described in equation 4.2 [27].

4.3.1 Pd-Cu alloy membranes preparation

> **Pd plating**

After surface activation, the 316L stainless steel substrates were plated with Pd by electroless plating technique. The plating solution consisted of $Pd(NH_3)_4Cl_2 \cdot H_2O$, 28% ammonia solution, and EDTA. An excess of ammonium hydroxide is necessary to stabilize the plating solution and maintain the pH at 10.

Anhydrous hydrazine, a reducing agent, was then added into the Pd plating solution when its temperature reached 60°C. During the immersion of the substrates some bubbling gases were observed due to the redox reaction [38].

At the end of plating step, the substrate was cleaned and dried. It appeared silver-like in color which is the indication of Pd larger. It was explained by several other research groups that the reaction occurred on the surface of the substrate, and preferentially around the Pd seeds. The occurrence was initiated by the reaction of hydrazine with hydroxide ion forming nitrogen gas and water with simultaneous release of electron. The electrons were transferred across the Pd island and used for reducing Pd^{2+} complex into Pd metal. The Pd metal was deposited onto the nuclei resulting in growth. Nitrogen and ammonia gases were concomitantly evolved as bubbles during the plating process. It obviously showed that the smooth surface was obtained resulting from Pd deposition onto the substrate surface until a certain thickness was developed [50].

In general, the thickness of Pd layer was measured by SEM. As seen from the images in Figure 4.6, the top surface became smooth and has a gray color on 316L stainless steel substrate [51].
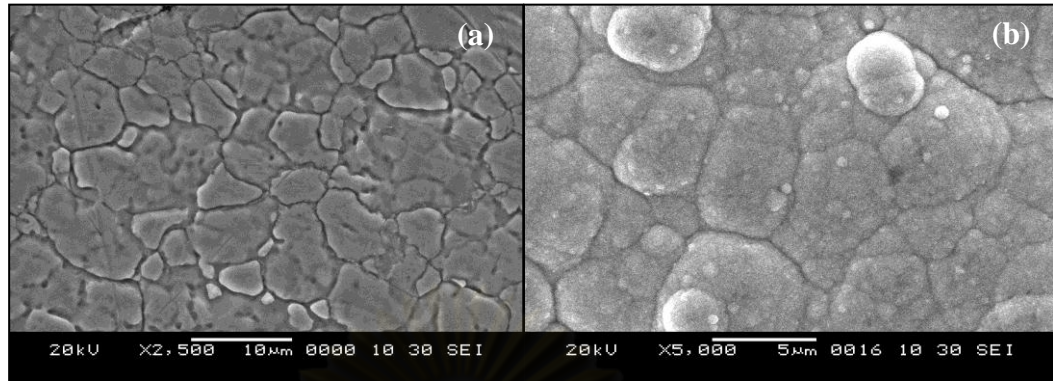
Figure 4.6 SEM images of (a) stainless steel substrate and (b) Pd layer deposited on 316L stainless steel substrate.

The successful preparation of Pd-Cu alloy membrane on 316L stainless steel substrates was showed the various composition; in weight% for the alloy membrane. The elemental mapping indicated that Pd and Cu were homogeneously distributed in the binary membrane.

Table 4.1 The thicknesses and compositions of Pd-Cu binary alloy membranes

Cu plating time(min)	Thickness (µm)	Weight% Pd-Cu		Atomic% Pd-Cu		Stoichiometric form
		Pd	Cu	Pd	Cu	
5	5.96	50.81	49.19	49.21	50.79	$Pd_{0.50}Cu_{0.50}$
4	5.14	58.35	41.65	60.97	39.03	$Pd_{0.60}Cu_{0.40}$
3	4.96	74.61	25.39	70.22	29.78	$Pd_{0.70}Cu_{0.30}$
2	4.52	86.15	13.85	79.65	21.35	$Pd_{0.80}Cu_{0.20}$
1	4.04	91.69	8.31	89.33	11.67	$Pd_{0.90}Cu_{0.10}$

During annealing of bimetallic layer at the initial stage of the treatment, some Cu atoms diffused into the Pd and vice versa. As diffusion process occurred, Cu atoms started to diffuse into the Pd rich phase through the interface faster than Pd atoms diffused into the Cu rich phase. This made the diffusion of Cu within the Pd rich phase was relatively fast. Schematically, the alloying process of Pd-Cu bi-layers took place as if a Cu layer, analog to a Cu atoms reservoir, disappeared at the expense of a Pd rich phase. The diffusion of Cu through the Cu/Pd-Cu interface led to the shifting of the Cu/Pd-Cu interface in the outer direction. Depending on

the amount of Cu deposited on top of the Pd layer different phases appeared during the homogenization of the alloy [52].

> **Characterizations (SEM/EDS and XRD)**

In the formation of the Pd-Cu membrane it was found that the atomic interdiffusion of Pd and Cu after a long-term annealing. The cross-sectional images over the Pd-Cu/SS membrane before annealing showed in Figure 4.7, it was found that the layers of Pd and Cu were separated.
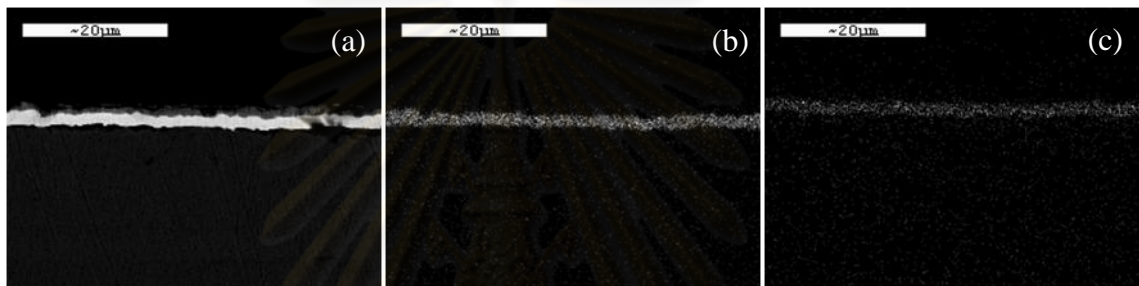
Figure 4.7 Cross-sectional SEM images of (a) Pd-Cu alloy membrane before annealing process, (b) elemental mapping of Pd and (c) elemental mapping of Cu.

Figure 4.8 showed elemental mapping of Pd-Cu binary alloy membrane after annealing process Pd and Cu metals were mixed and successful diffusion of the Pd-Cu alloy membrane. The elemental mapping of Pd and Cu indicated the homogeneous distribution of Cu and Pd.
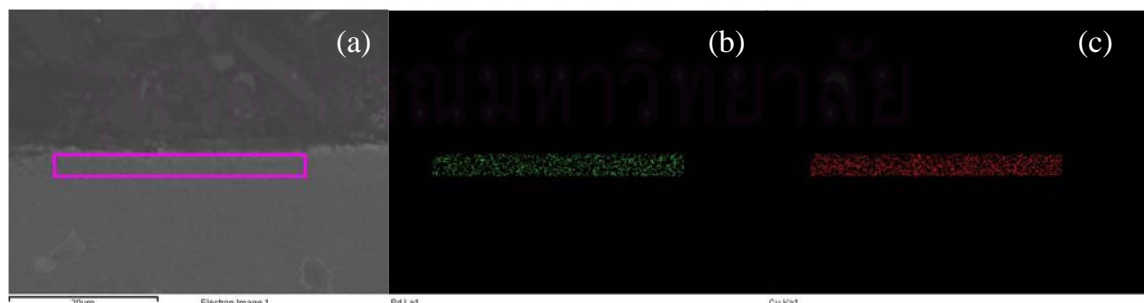
Figure 4.8 Cross-sectional SEM images of (a) Pd-Cu alloy membrane, (b) elemental mapping of Pd and (c) elemental mapping of Cu.

From the cross-sectional SEM images of the Pd-Cu alloy membrane, it was found that the highly uniform and have a good adhesion to the substrate. For the EDS spectra which showed the elementary of the characteristic x-ray emission from Pd-Cu alloy membrane on 316L stainless steel substrates after annealing process are showed in Figure 4.9 it was found that the contents of Pd and Cu were at 60.97% and 39.03% (atomic%) of the whole Pd-Cu alloy membrane.
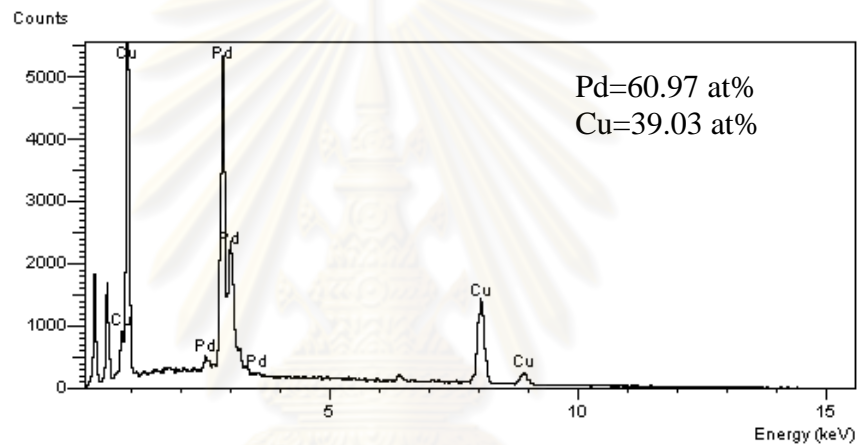
Figure 4.9 The EDS spectra of Pd-Cu binary alloy membrane.

Figure 4.10 XRD diffractrogram showed peaks of Pd-Cu binary alloy membranes in composition of $Pd_{0.50}Cu_{0.50}$, $Pd_{0.60}Cu_{0.40}$ and $Pd_{0.70}Cu_{0.30}$, indicated that the Pd and Cu metals were mixed successfully. After annealing, it was found that the diffraction peaks of Pd-Cu alloy membranes were confirmed at 2θ position = 41.2°, 48.9° and 72.1° which were PdCu(111), PdCu(200) and PdCu(220), respectively. The Pd-Cu alloy membrane was confirmed to the metal alloying. The phase structure of pure Pd and Cu were changed to Pd-Cu alloy structure [53].
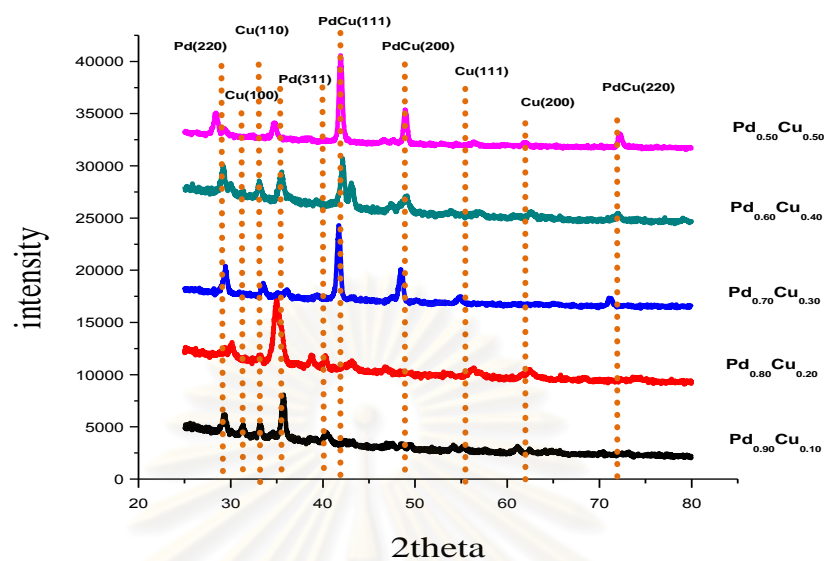
Figure 4.10 XRD diffractograms of Pd-Cu binary alloy membranes after annealing.

4.3.2 Pd-Ag alloy membranes preparation

Alloying Pd with Ag not only suppresses the critical temperature for hydrogen embrittlement, but also increases the permeability of the alloy membrane. Pd membranes are required to have high hydrogen permeance, good thermal and mechanical stability and permeation selectivity. Pure Pd membranes, however, suffer from hydrogen embrittlement caused by the α to β phase transformation when the temperature is lower than the critical temperature of 300°C [6].

All of these studies achieved some degree of alloy formation, as indicated by an increase in the hydrogen permeation following the heat treatment. For the Pd-Ag system, the membrane formation was mixed in Pd and Ag with uniform compositions. The diffusion treatment was accomplished at a temperature of 900°C under an argon atmosphere. Over an Ag composition range of 0-50wt%, this approach resulted in uniform Pd and Ag compositions throughout the membrane [45].

The surface morphology and composition of the electrodeposite were influenced by current density, and Ag concentration in the bath. The increase of

current density made the surface morphology of the electrodeposit to be finer and smoother alloy membrane. The Ag concentration in the bath should be controlled precisely because the membrane growth of Ag can occur easily because of the increase of limiting current density [54].

It was found that the phase and crystal structure of the alloys depend on the alloy compositions. A phase structure of Pd-based alloy membranes were consisting of both body centered cubic (bcc) and face centered cubic (fcc) phase structure. However, the atomic radius of Pd, Ag and Cu was 0.137, 0.144 and 0.128 nm which were similar and the Pd, Ag, Cu metal can replaced in the alloy structure. The possibility of Ag and Cu combination in Pd-based alloy membrane was found that from addition of Ag and Cu metals, both of this metal substituted in Pd atoms based on membrane.

The thicknesses and compositions of Pd-Ag alloy membrane were determined by cross-sectional SEM images were showed in Table 4.2.

Table 4.2 The thicknesses and compositions of Pd-Ag binary alloy membranes

Ag plating time(sec)	Thickness (μm)	Weight% Pd-Ag		Atomic% Pd-Ag		Stoichiometric form
		Pd	Ag	Pd	Ag	
5	5.20	50.21	49.79	49.45	50.55	$Pd_{0.50}Ag_{0.50}$
4	4.80	60.67	39.33	63.43	36.57	$Pd_{0.60}Ag_{0.40}$
3	4.32	70.61	29.39	67.22	32.78	$Pd_{0.70}Ag_{0.30}$
2	3.68	82.15	17.85	79.46	20.54	$Pd_{0.80}Ag_{0.20}$
1	3.20	90.69	10.31	90.57	9.43	$Pd_{0.90}Ag_{0.10}$

➢ **Characterizations (SEM/EDS and XRD)**

Before and after annealing process, the Pd-Ag alloy membranes were measured by SEM/EDS to confirm the metal distribution and showed a homogeneous alloying. The EDS elemental mapping of Pd and Ag were separated before annealing process as showed in Figure 4.11. After annealed, two metals were mixed homogeneously and have highly distribution of Pd and Ag into the Pd-Ag alloy membrane as seen in Figure 4.12.
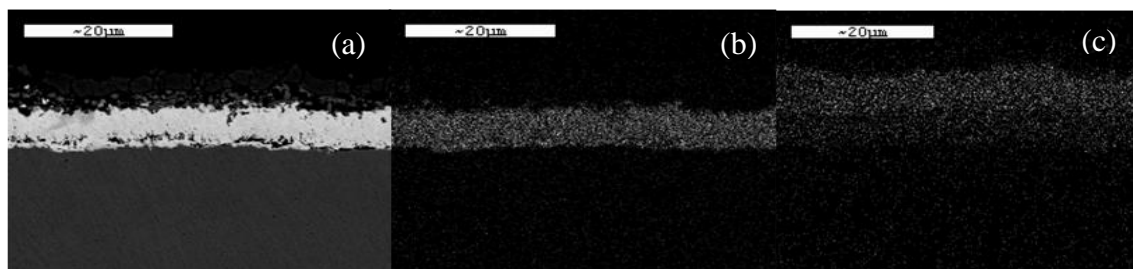
Figure 4.11 Secondary electron images before annealing of (a) Pd-Ag alloy membrane, (b) elemental mapping image for Pd and (c) for Ag.
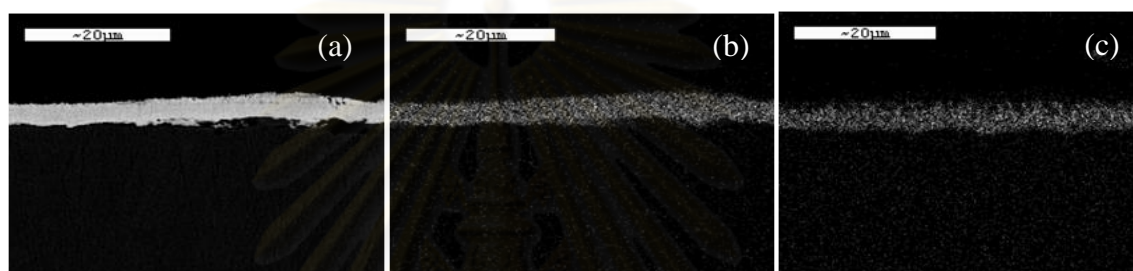
Figure 4.12 Secondary electron images after annealing of (a) Pd-Ag alloy membrane, (b) elemental mapping image for Pd and (c) for Ag.
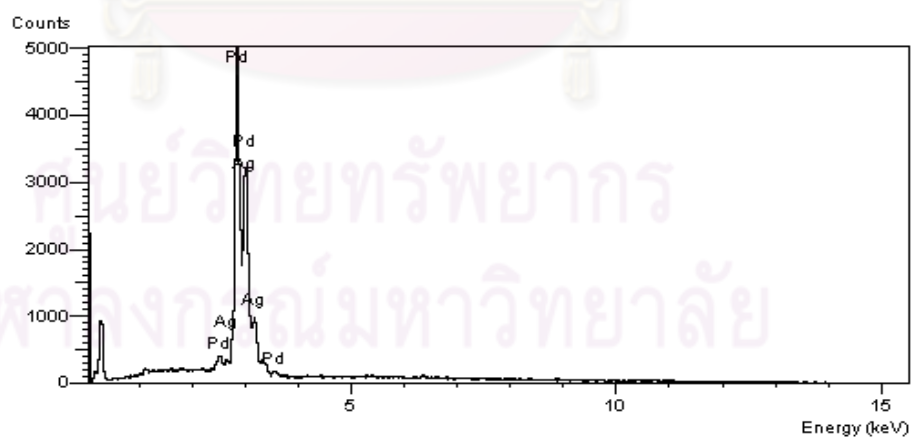
Figure 4.13 EDS spectrum of Pd-Ag alloy membrane.

Figure 4.13 showed EDS spectrum of Pd-Ag alloy membrane on the substrate after annealing, it was found that the content of Pd and Ag was at 67.22%

and 38.78% (atomic%) of the whole Pd-Ag alloy membrane. The spectra were confirmed the Pd and Ag metals, have highly distribution in the alloy membrane.
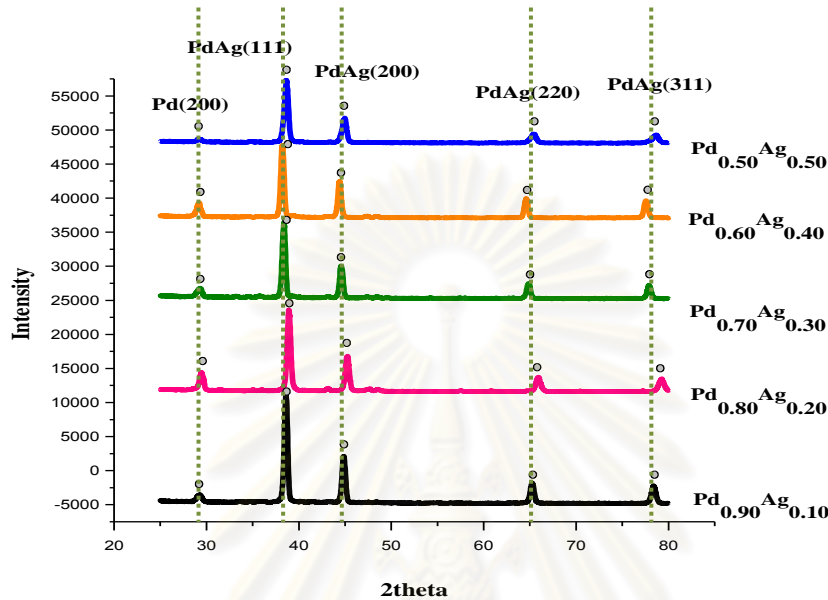
Figure 4.14 XRD diffractrograms of Pd-Ag binary alloy membrane**s.**

From XRD diffractrograms of Pd-Ag alloy in various compositions, it was found that the peaks at $2\theta = 38.1°$, $44.9°$, $65.3°$ and $78.3°$ correspond to the existing of Pd-Ag alloy, as labeled in Figure 4.14 [55].

The annealing conditions were used for the Pd-Ag layers in the thickness range of 3.0-5.0 μm. The annealing conditions were used for the Pd-Ag layers in the thickness range of 3.0-5.0 μm. The alloy of Pd and Ag structures obtained after sequential electroplating was studied. The disappearance of the pure Pd and pure Ag reflections at 2θ position = 29.45, 35.58, 46.94, 62.84, 71.06 and 38.78, 45.85, 67.64, 81.53, respectively. After annealing, the compositions could be accurately determined from the positions of the alloy reflections from the analysis of XRD measurement results. The obtained Pd-Ag alloy peak positions are corresponded to Nair R. *et al.* which each compositions were confirmed the existing of Pd-Ag alloy [56].

4.3.3 Pd-Ag-Cu alloy membranes preparation

It was reported that the addition of Cu or Ag to the Pd films improved the membrane, making it suitable to be utilized below 300°C, at the same time maintaining the extremely high selectivity and reducing the hydrogen permeability [39]. Jun and Li have prepared a thin Pd composite membranes with high hydrogen selectivity. These ternary alloys have been made to examine large numbers of alloys because such efforts would required extremely large resources and promise an uncertain outcome [27,28]. Kamakoti and Sholl did some calculation on the ternary alloys and found that they can give a higher hydrogen flux than comparable for Pd-Cu and Pd-Ag binary alloys. In our work, ternary alloys of composition $Pd_xM_yCu_{1-x-y}$ with x>0.50 and y<0.05 (in at%) were controlled and investigated. M is a third metal for adding in the alloy membrane. The Pd-Ag-Cu ternary alloy membranes were varied by Pd electroless plating, followed by Ag and Cu electroplating. Three compositions of material, $Pd_{0.80}Ag_{0.05}Cu_{0.15}$, $Pd_{0.85}Ag_{0.05}Cu_{0.10}$ and $Pd_{0.90}Ag_{0.05}Cu_{0.05}$ of ternary alloy membrane were obtained. It was found that the presence of other metals as Ag, Ru, Cu and Au, at specific concentrations, also enhance the hydrogen permeation flux with no negative effects on its selectivity [57]. The thickness of Pd-Ag-Cu alloy membrane was about 6-7 µm in average from SEM characterization. The weight% and atomic% composition of alloy membranes are showed in Table 4.3.

Table 4.3 The weight% and atomic% of Pd ternary alloy membranes

	Composition (wt%)			Composition (at%)			Stoichiometric form
	Pd	Ag	Cu	Pd	Ag	Cu	
A	79.15	5.13	15.72	78.18	5.02	16.80	$Pd_{0.80}Ag_{0.05}Cu_{0.15}$
B	85.12	4.67	10.21	85.23	5.10	10.67	$Pd_{0.85}Ag_{0.05}Cu_{0.10}$
C	89.82	4.93	5.35	90.12	4.87	5.01	$Pd_{0.90}Ag_{0.05}Cu_{0.05}$
D	85.67	4.68	9.65	84.78	5.21	10.01	$Pd_{0.85}Ag_{0.05}Cu_{0.10}/Cr_2O_3$

➢ **Characterizations (SEM/EDS and XRD)**

In this part of the work, tri-layers of Pd, Ag and Cu including alloy were investigated by using XRD and EDS analysis. XRD and EDS analysis would be useful to calculate bulk composition of the samples and also to estimate the amount of Pd-Ag-Cu deposited with varied plating time. The formation of a substrate by the electroless and electroplated deposition would allow for the production of a membrane having a thinner hydrogen selective layer.
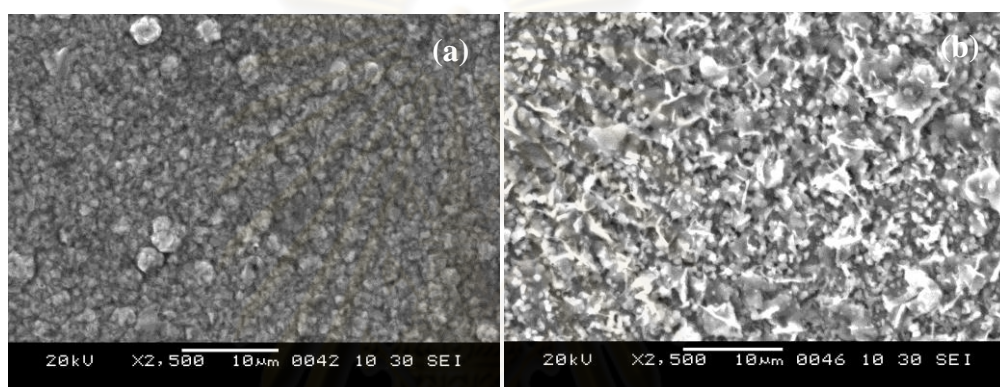
Figure 4.15 Surface images of (a) Pd-Ag-Cu layer before annealing process and (b) after annealing process.

Figure 4.15 showed the surface images of Pd-Ag-Cu before and after annealing process. This indicated that the gain size of Pd-Ag-Cu ternary alloy membrane after annealing has developed. We attempted to control the deposition rates of each metal layer by optimizing the composition and plating time.
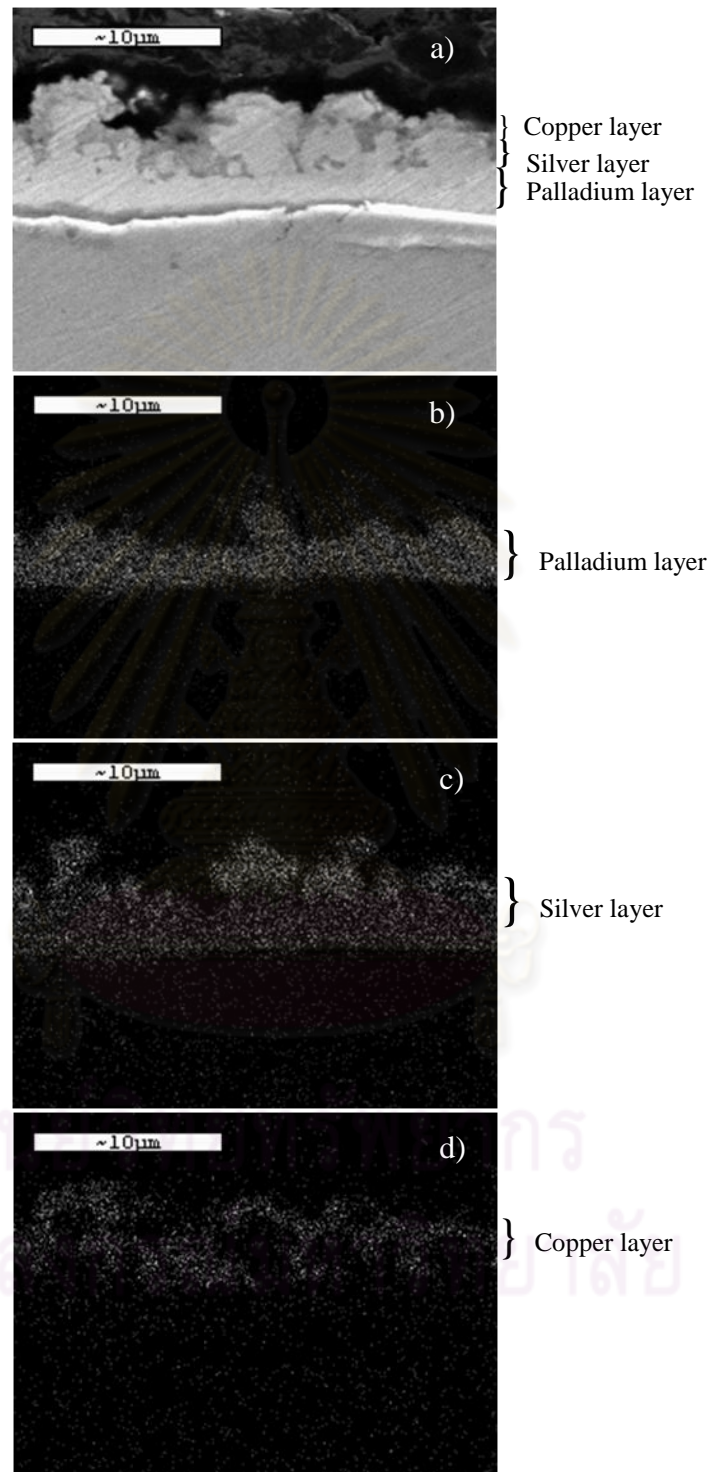
Figure 4.16 Cross-sectional SEM images of (a) Pd-Ag-Cu ternary alloy membrane before annealing process, (b) elemental mapping of Pd layer, (c) elemental mapping of Ag layer and (d) elemental mapping of Cu layer.

The cross-sectional SEM images before annealing process of Pd-Ag-Cu was deposited on the substrate which was analyzed by SEM and EDS. It was found that the Pd, Ag and Cu metals were separate layers are showed in Figure 4.16. After annealing at 1100°C for 20 hours in argon atmosphere, the cross-sectional of the layer showed a homogeneous and continuous of alloy membrane. EDS spectra of Pd-Ag-Cu ternary alloy membrane was performed at various points in the layer to determine if a uniform alloy was produced by annealing. From EDS spectra, the energy of each metals element splited in various composition as seen in Figure 4.17. It was found that the contents of Pd, Cu and Ag were 78.18%, 5.02% and 16.80% (atomic%) of the whole Pd-Ag-Cu alloy membrane.
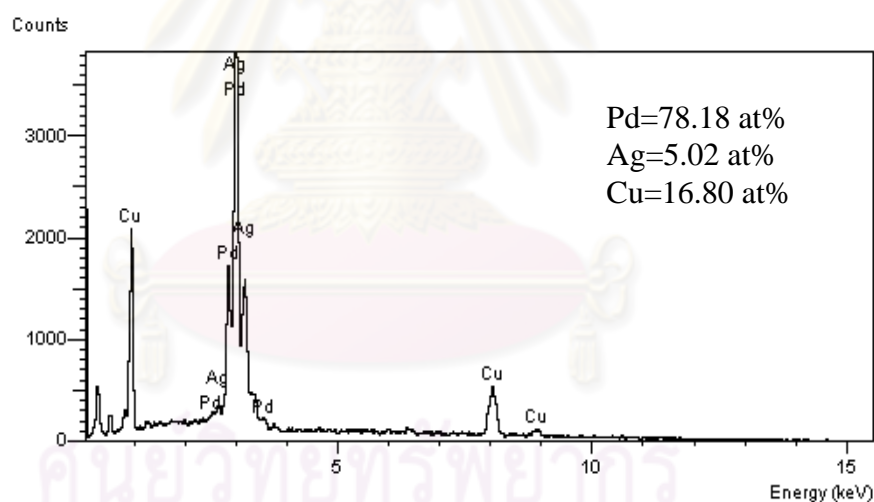
Figure 4.17 EDS spectra of Pd-Ag-Cu alloy membrane**.**

The XRD patterns of Pd-Ag-Cu ternary alloy membrane after annealing process are showed in Figure 4.18. In order to optimize the alloy formation, the samples were controlled at different deposition time to have different alloy structures and compositions of the membranes. After annealing process, it was found that the phase structures of Pd-Ag-Cu ternary alloy membranes were changed are showed PdAgCu(111), PdAgCu(200), PdAgCu(220) and PdAgCu(311) in the alloy

membrane layer. The solution diffusion mechanism of metal alloy membrane was used to the thermal and time for metal mixing thoroughly the membrane and have a successfully of the metal alloying [58]. In the alloy membranes have a many Pd therefore after annealing at high temperature it was found that the Pd metals were remained in the alloy membranes.
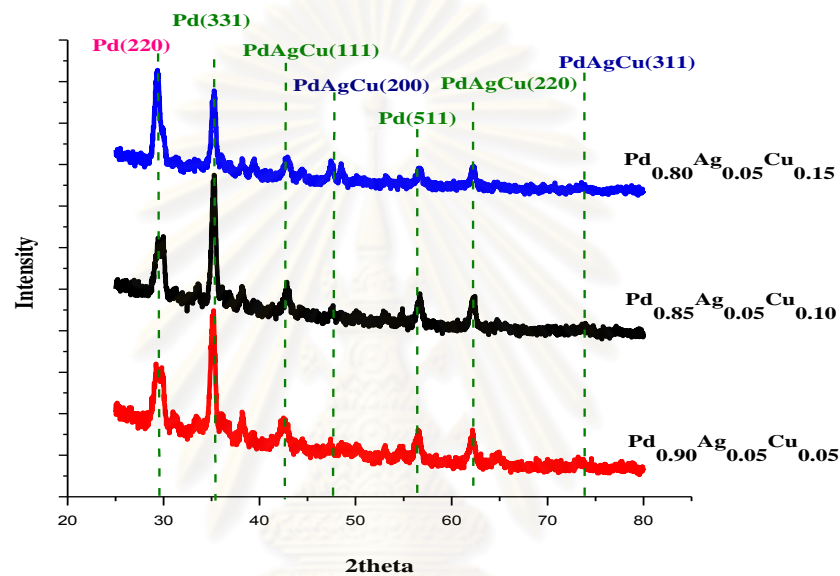
Figure 4.18 XRD diffractrograms of Pd-Ag-Cu ternary alloy membranes.

Figure 4.19 showed the cross-sectional elemental mapping of Pd-Ag-Cu sequential deposits obtained by the electroless plating and electroplating techniques. It was found that all three metals in layer were well distributed in the whole membrane thickness. The deposition of alloy membranes shows uniform and smooth surface image.
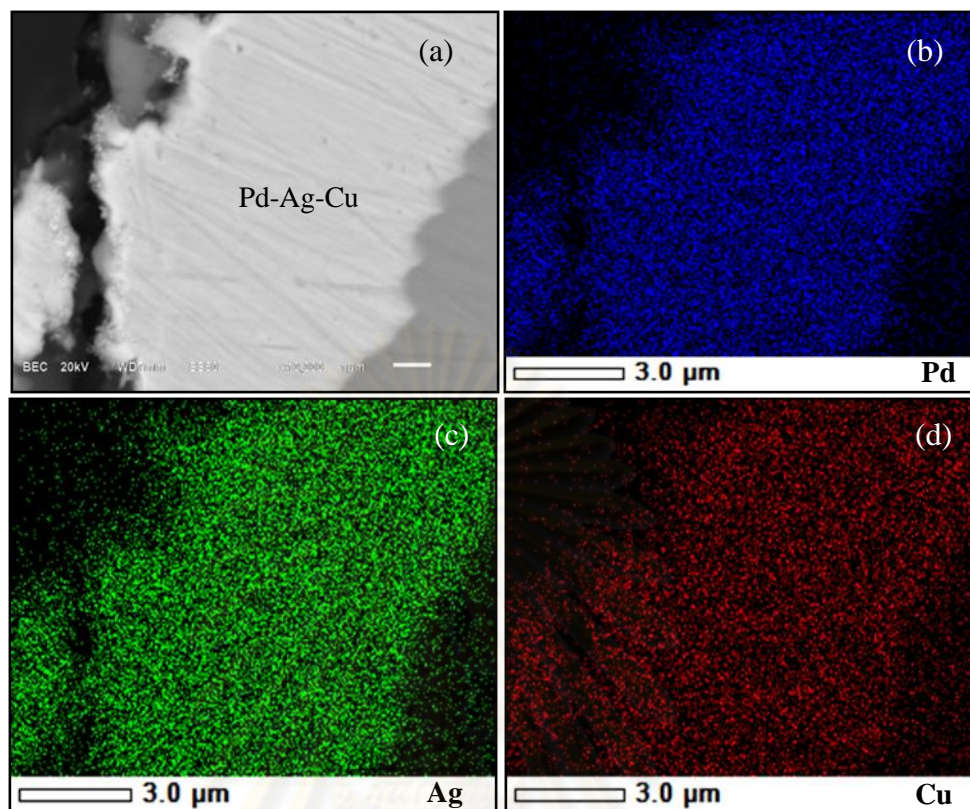
Figure 4.19 Cross-sectional SEM images after annealing of (a) Pd-Ag-Cu membrane at 1100°C for 20 hours, (b) elemental mapping of Pd, (c) elemental mapping of Ag and (d) elemental mapping of Cu.

4.4 Mechanicals properties measured by Nanoindentations

Mechanical properties, such as hardness and ductility, change a dislocations are eliminated and the metal's crystal lattice is altered. On heating at specific temperature and cooling it is possible to bring the atom at the right lattice site and new grain growth can improve the mechanical properties. Ag in an alloying of Cu-Pd alloy also improves their strength. In this case, Pd-Ag-Cu alloys are of interest as a functional material for a wide range of applications. Pd and Pd-alloy film have reduced material cost and provides a structure possessing both higher hydrogen flux and better mechanical properties [37].

For mechanical properties, the CSM™ nanoindentor was used to determine the hardness of the Pd-Ag-Cu membrane thin films. In the measurements a Berkovich-type diamond indenter tip was used and the maximum indenter depth

penetration was kept less than 10% of the film thickness to prevent the substrate effects. For Pd, Pd-Ag, Pd-Cu and Pd-Ag-Cu thin films, the maximum values of hardness are found at 3.57, 5.51, 8.41 and 7.23 GPa, respectively, as showed in Figure 4.20. This result was corresponded to Sabina K. *et al.* for an improvement of the mechanical properties of the material. As seen in the graph below, the hardness of all groups of samples can be ordered as Pd-Cu > Pd-Ag-Cu > Pd-Ag > Pd. It was found that Pd-Cu alloy membrane has the highest hardness value and the hardness of Pd-Ag-Cu is in between the Pd-Ag and Pd-Cu binary alloy membrane. However, the Pd-Ag-Cu alloy membrane was a good mechanical properties for membrane separation and this result supports for improvement of alloying [47].
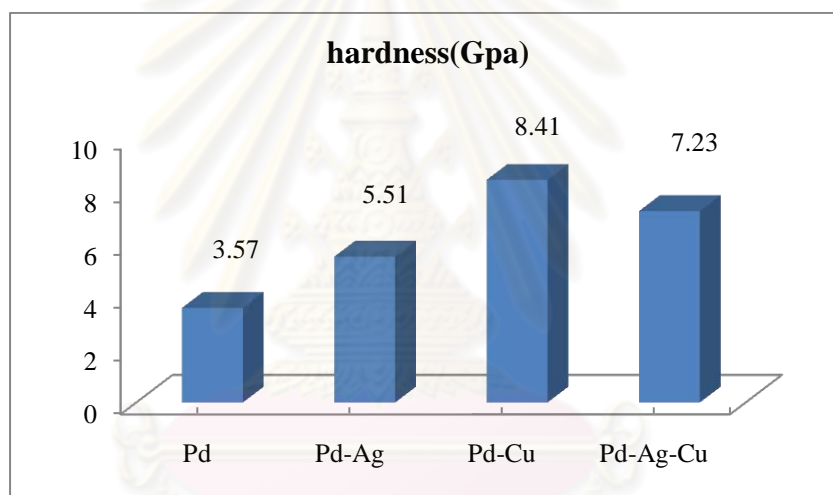
Figure 4.20 Hardness measured by nanoindentation.

4.5 Preparation of intermetallic diffusion barriers

In this study chromium oxide was constructed to be the diffusion barriers on the 316Lstainless steel substrate. The most suitable condition for prepared Cr electroplating followed by oxidation step was at 600°C for 6 hours. It was found that the Cr_2O_3 intermetallic diffusion barrier prepared by electroplating well in shielding the Pd-alloy layer. The Cr_2O_3 intermetallic diffusion structure on the substrate is showed in Figure 4.21.
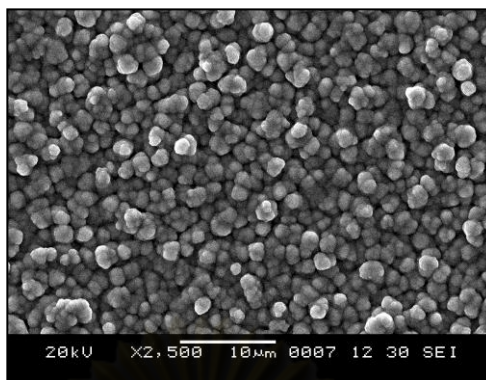
Figure 4.21 SEM image of the surface of Cr-thin film by electroplating after oxidizing at 600°C for 6 hours.

From the results in previous work, it was found that the Cr_2O_3 intermetallic diffusion barrier are suitable oxidation temperature was therefore considered to be at 600°C for 6 hours [2].

4.6 Performance testing of Pd, Pd-Cu, Pd-Ag and Pd-Ag-Cu membranes

The permeation of hydrogen gas was measured at different temperature and pressures. This was carried out at 350, 400, 450 and 500°C for different pressures at 0.5-3.0 atm. The PSS was used as the substrate for hydrogen permeation flux test. The Pd-Ag-Cu membranes were plated on the PSS with the Cr_2O_3 intermetallic diffusion thin films. Preliminary testing for dense Pd-Ag-Cu membranes was carried with helium gas at room temperature for different pressures up to 3 atm. It was found that there is no gas permeation. The samples were put in pressure test housing crafted of 316L stainless steel and graphite gaskets were used to make gastight seals. Single gas permeation experiments with hydrogen and helium permeation flows were measured by soap bubble flow meter.

The thickness of the Pd-based layer was calculated by SEM image averages 6-7 µm. After hydrogen permeation testing it was found that the membranes were not embrittle and have a good stability in hydrogen atmosphere.

A steady-state counter diffusion method, using gas chromatographic analysis, was used to measure the permeability and selectivity of the Pd-based membrane for hydrogen separation. The method consisting of a diffusion cell

designed to allow permeation of two different gases through a membrane or porous sample. The membranes were evaluated for hydrogen separation by conducting permeability measurements with hydrogen and helium at various temperatures and transmembrane pressure differentials.

The above experiment showed that the optimal heat treatment of a Pd-Ag-Cu alloy differs considerably from that of a conventional alloy. Furthermore, this temperature depends on the alloy composition. For binary Pd-Cu, Pd-Ag and ternary Pd-Ag-Cu heat treatment was 750, 900 and 1100°C, respectively.

Our results using a Pd-Ag-Cu/PSS membrane indicated that the Pd-Ag-Cu ternary alloy exhibits a promising behavior for hydrogen separation. As the temperature and feed side pressure of Pd and Pd-based alloy membrane were increased the permeation flux was increased. The membrane presents a hydrogen flux of $Pd_{0.85}Ag_{0.05}Cu_{0.10}$ at about 5.29 $m^3m^{-2}s^{-1}$ at 500°C and feed side pressure of 3.0 atm. It was found that the high hydrogen permeability and has a high resistance, the temperature and pressure were increased, the hydrogen permeation was increased.

From graphs, the hydrogen flux is linearly proportional to the pressure difference across the membrane at each temperatures. Figure 4.22-4.23 showed the plot of hydrogen flow rate. At each temperature, hydrogen permeation flux increased with an increasing pressure difference. At higher temperatures more hydrogen permeation depended on both temperature and the pressure differences in tube sides. The relationship between the hydrogen permeation flux and the square root of pressure difference ($P^{0.5}-P_0^{0.5}$) was plotted as in Figure 4.24 which showed a linear relationship between the hydrogen flux and the difference of the square root of pressure.
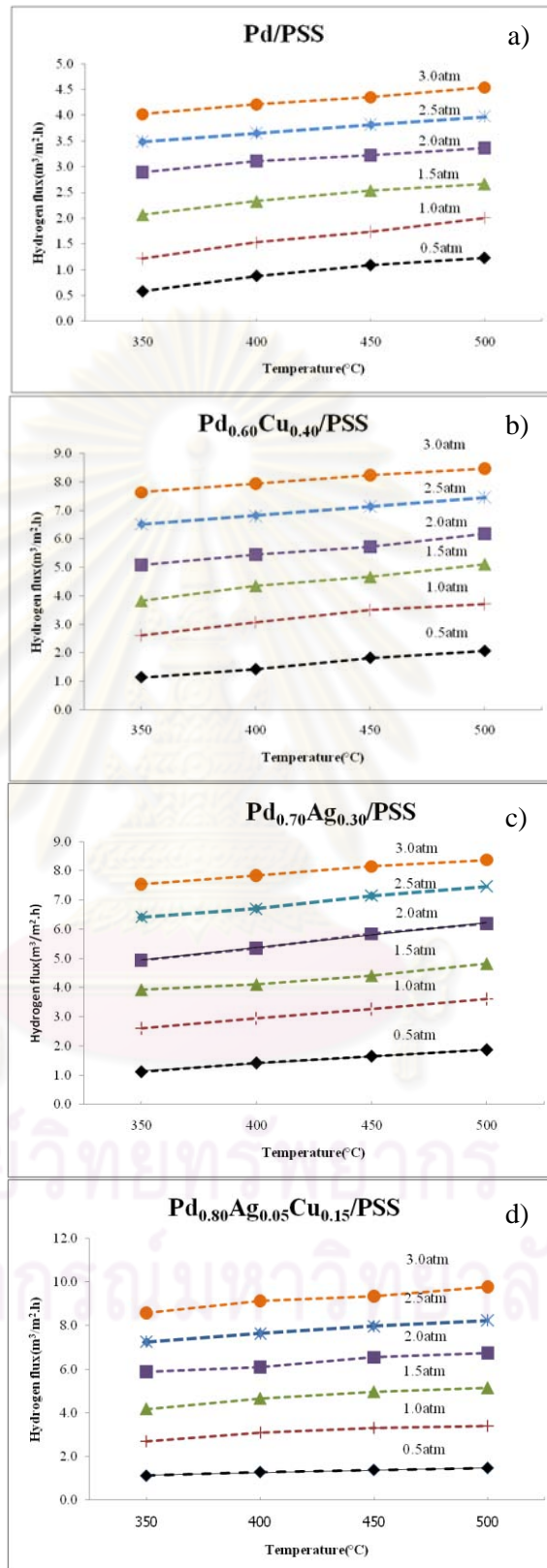
Figure 4.22 The relationship between temperature and pressure through Pd-based membranes in hydrogen permeation for (a) Pd/PSS, (b) $Pd_{0.60}Cu_{0.40}$/PSS, (c) $Pd_{0.70}Ag_{0.30}$/PSS, (d) $Pd_{0.80}Ag_{0.05}Cu_{0.15}$/PSS.
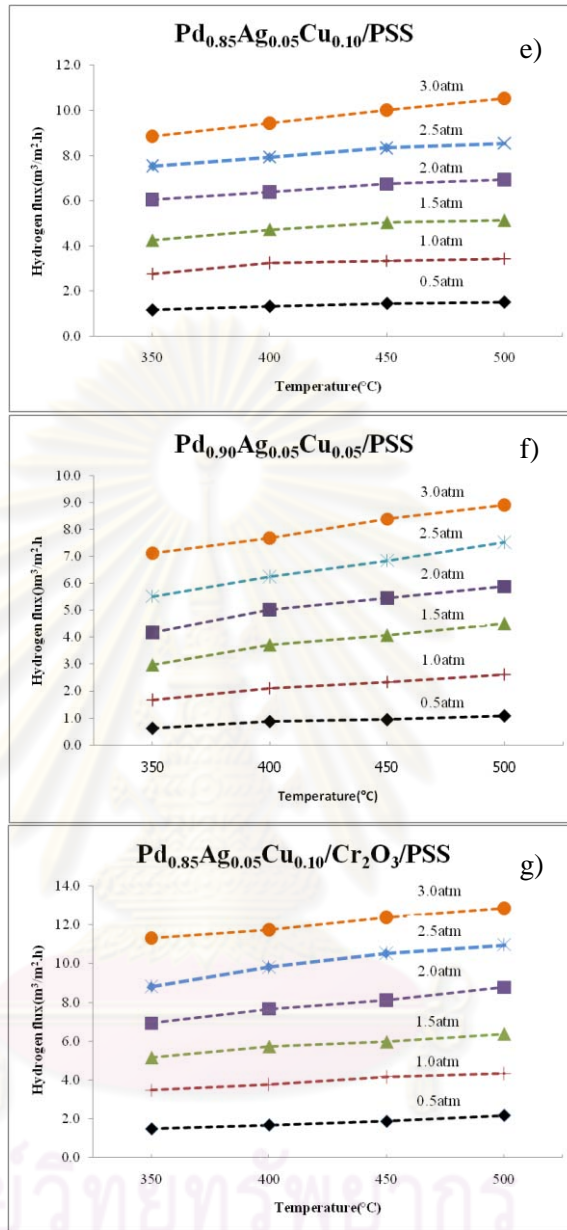
Figure 4.23 The relationship between temperature and pressure through Pd-based membranes in hydrogen permeation for (e) $Pd_{0.85}Ag_{0.05}Cu_{0.10}$/PSS, (f) $Pd_{0.90}Ag_{0.05}Cu_{0.05}$/PSS and (g) $Pd_{0.85}Ag_{0.05}Cu_{0.10}$/$Cr_2O_3$/PSS.

The hydrogen flux that obtained in mixtures of hydrogen with other gases can be influenced by several factors. It can reduce either the effective hydrogen partial pressure difference or the dissociative adsorption of hydrogen on the Pd-based membrane surface, including: (i) hydrogen dilution on the feed side by the presence of other gas components, (ii) hydrogen depletion of the bulk feed due to hydrogen removal along the length of the membrane module, (iii) the build-up of a hydrogen-depleted layer adjacent to the membrane surface due to gas phase mass transport limitation, (iv) possible competitive adsorption of other gas components on the membrane surface. The systematic permeation studies are performed in the following to separate the different contributions [39].

The hydrogen permeation through the dense metallic film increases substantially with an increasing temperature. As a result, the separation factor increases with increasing temperature unless there is a crack formation due to cycling or hydrogen embrittlement.

The permeation rate of hydrogen through Pd-based alloys can primarily be increased by decreasing the film thickness. The hydrogen permeation flux were measured not only the pressure difference but also the temperature were varied from 1-3 atm and 350-500°C, respectively.

The hydrogen permeation also showed that the mechanism of hydrogen gas diffusing through the bulk of Pd-alloy layer was the solution-diffusion mechanism. In this study, hydrogen gas was used to measure after no helium flux testing and it could be detected at pressure difference at 1 atm.

In this studied, the hydrogen permeation and mechanical properties can be improved from those Pd-Ag and Pd-Cu alloy membrane. In various compositions of Pd-Ag-Cu alloy membranes, it was found that the difference hydrogen permeation which increased the temperature and pressure, hydrogen permeation was increased. However, the Pd ternary alloy membranes have more advantage than the Pd binary alloy membrane and Pd membrane in hydrogen separation and have a low cost.
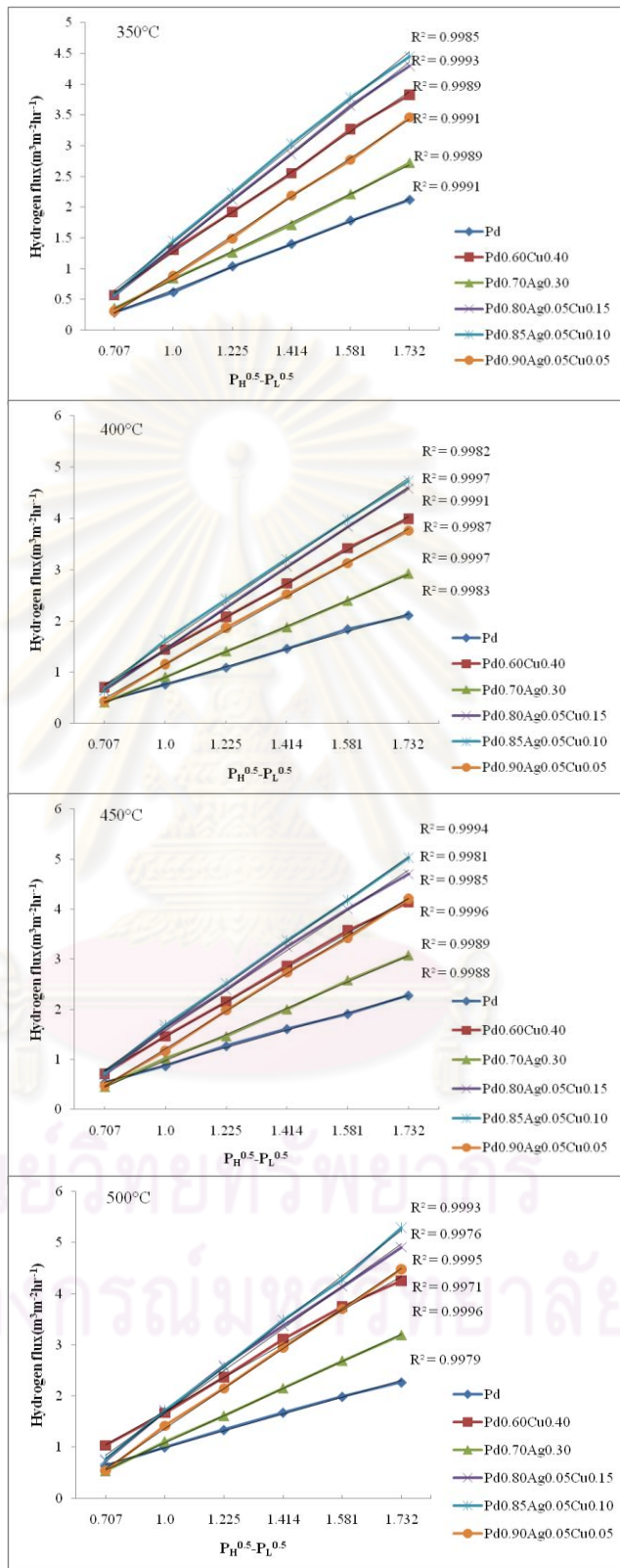
Figure 4.23 Sievert's law plots of Pd-based membrane at various temperatures
(a) 350°C, (b) 400°C, (c) 450°C and (d) 500°C.

Hydrogen permeates through solid metals in atomic form by solution-diffusion mechanism. Hydrogen molecules first adsorb on the metal surface and are dissociated into atoms which then diffuse through the bulk metal under a concentration gradient. After passing through the bulk metal, the hydrogen atoms recombine into hydrogen molecules at the opposite metal membrane surface and the molecular hydrogen gas exits from the surface to the gas phase. The diffusive flux of hydrogen through a bulk metal membrane of thickness L is generally described by Sievert's law [59].

Prior to the hydrogen permeation tests, the Pd-based membrane was heated in helium at a rate of about 4°C/min. The hydrogen permeation flux and hydrogen permeance of dense Pd and Pd alloy membranes were calculated according to the following equation:

$$hydrogen\ permeation\ flux\ \left(\frac{m^3}{m^2h}\right) = \left(\frac{flow\ rate\ of\ hydrogen\ gas\ \left(\frac{ml}{min}\right)}{active\ surface\ area\ (cm^2)}\right) \times 0.6$$

$$hydrogen\ permeance\ \left(\frac{m^3}{m^2hatm^{0.5}}\right) = \left(\frac{hydrogen\ permeation\ flux\ \left(\frac{m^3}{m^2h}\right)}{P_{H_2\ at\ shell\ side}^{0.5} - P_{H_2\ at\ tube\ side}^{0.5}\ (atm^{0.5})}\right)$$

Variety of porous substrates has been used for dense Pd-alloy membranes. A lot of studies describe different methods to fabricate such composite membranes. The commonly used methods are electroless plating and electroplating. The thin Pd and Pd-alloy layer were prepared on the surface or inside the pores of porous substrates. The linear relationship between hydrogen permeation flux and the square root of pressure difference $(P_H^{0.5}-P_L^{0.5})$ indicates that the hydrogen permeation flux follows the Sievert's law [51,52] confirming the hydrogen diffusion through Pd-based membrane as the rate determining step. It was found that the hydrogen permeation gave permeation flux as low as that obtained from Pd membrane without the diffusion barriers. The hydrogen permeation flux of Pd and Pd-based alloy membranes increased in the order, $Pd < Pd_{0.70}Ag_{0.30} < Pd_{0.60}Cu_{0.40} < Pd_{0.90}Ag_{0.05}Cu_{0.05} < Pd_{0.80}Ag_{0.05}Cu_{0.15} < Pd_{0.85}Ag_{0.05}Cu_{0.10}$. This test result was correspond with the result which added ~4 wt% Ag to improve permeability of Pd-Cu by 20-25% [60].

The results of hydrogen permeance in Pd-based alloy membranes were showed in Table 4.4. It was found that $Pd_{0.85}Ag_{0.05}Cu_{0.10}$ alloy membranes with diffusion barriers give higher hydrogen permeance than $Pd_{0.85}Ag_{0.05}Cu_{0.10}$ alloy membrane without the barrier. Without the barriers, the Pd ternary alloy membrane has a higher hydrogen permeance. From coating Pd-based alloy on the substrates, these results were correspond with Tarditi, A.M. study [58]. Provided that the Pd-based alloy membranes had intermetallic diffusion barrier, hydrogen permeation flux would be increased. Chromium oxide used as intermetallic diffusion barrier effectively prevented the intermetallic diffusion and gave highly hydrogen permeation flux. After post hydrogen permeation testing the metal based alloy membrane was fairly uniform and was not hydrogen embrittlement [60, 61].

Table 4.4 Hydrogen permeance with various Pd-based alloy membrane**s**

Membrane	Hydrogen permeance $m^3(STP)/(m^2.hr.atm^{0.5})$			
	Temperature(°C)			
	350	400	450	500
Pd/PSS	2.09	2.11	2.28	2.27
$Pd_{0.60}Cu_{0.40}$/PSS	3.83	3.97	4.14	4.25
$Pd_{0.70}Ag_{0.30}$/PSS	2.72	2.93	3.08	3.19
$Pd_{0.80}Ag_{0.05}Cu_{0.15}$/PSS	4.29	4.58	4.69	4.91
$Pd_{0.85}Ag_{0.05}Cu_{0.10}$/PSS	4.45	4.73	5.03	5.29
$Pd_{0.90}Ag_{0.05}Cu_{0.05}$/PSS	3.46	3.76	4.21	4.48
$Pd_{0.85}Ag_{0.05}Cu_{0.10}/Cr_2O_3$/PSS	5.67	5.89	6.21	6.44

The addition of Ag and Cu atoms in the Pd membrane for hydrogen separation can improve a hydrogen permeation and mechanical properties to the ternary metal alloy membrane. In various compositions of Pd-based alloy membranes, it was found that the hydrogen permeation was different. The Pd-Ag-Cu alloy membranes were added 5-15% of Cu and 5% of Ag, it was found that 10% of Cu added to Pd-based alloy membrane gave a high hydrogen permeation and had a good advantage for hydrogen separation [60].

CHAPTER V

SUMMARY AND SUGGESTIONS

In this study, electroless and electroplating deposite of Pd, Cu and Ag metals were used to fabricate the Pd-based alloy membranes. It was found that as the plating time increased, the thickness of metal layer was increased. Hence, the alloy composition could be controlled. The Pd-based alloy membrane with Ag and Cu was successfully formed. Both binary and ternary alloy materials had a good adhesion and uniformity. The SEM and EDX analysis after annealing the membrane, showed highly uniform distribution throughout the cross-section of both types of alloy membranes.

The binary and ternary alloy membrane composition was deposited on the substrate and the metals composition of the alloy membrane was controlled by chemical composition and deposition time. The effect of composition and deposition time for plating at various compositions in the metals alloy membrane was investigated. In addition, the mechanical properties which were results from addition of the third metal to improve the Pd-based alloy membranes had been characterized. It was found that the mechanical properties had a good hardness appropriately applied the alloy membrane for hydrogen separation.

The hydrogen permeation was carried out between 350-500°C and 0.5-3.0 atm. It was found that the hydrogen permeation flux obtained from the Pd-based alloy membrane with the diffusion barriers was higher than that without. The film acts as selective separation barrier for hydrogen separation. This Pd-alloy membrane was tested and characterized for hydrogen separation. The different permeation behavior for Pd-Ag-Cu membrane could be explained with different membrane thickness, structure, surface composition and morphology. From permeability studies with pure gases, it was found that a new Pd-Ag-Cu alloy membrane had a very high permselectivity for hydrogen and permselectivity increases with increasing operating temperature and pressure.

The advantages of Ag additional atoms in Pd-based alloy membranes were prevention of the hydrogen embrittlement and gained higher hydrogen permeation. Furthermore, the advantages of Cu additional atoms in Pd-based alloy membrane improved the mechanical properties of membrane. It could also give a good chemical resistance from poisoning H_2S and high hydrogen permeability.

The membrane showed the complete hydrogen selectivity and no decrease of hydrogen flux. Moreover, it is no intermetallic diffusion between Pd-alloyed membrane and the support from the membrane analysis after hydrogen testing. Therefore, the membrane had potential for application at elevated temperature for hydrogen separation and also used in membrane reactor for production and separation.

5.1 Further works

5.1.1 Test long-term stability of hydrogen permeation flux for Pd-Ag-Cu ternary alloy membrane.

5.1.2 Application for used in membrane reactor tubes.

References

[1] Nam, S.E.; and Lee, K.H. Preparation and Characterization of Palladium Alloy Composite Membranes with a Diffusion Barrier for Hydrogen Separation. **Industrial & Engineering Chemistry Research** 44 (2005): 100-105.

[2] Samingprai, S.; Tantayanon, S. and Ma, Y.H. Chromium oxide intermetallic diffusion barrier for palladium membrane supported on porous stainless steel. **Journal of Membrane Science** 347 (2010): 8-16.

[3] Bosko, M.L.; Ojida, F.; Lombardo, E.A.; and Cornaglia, L.M. NaA zeolite as an effective diffusion barrier in composite Pd/PSS membranes. **Journal of Membrane Science** 331 (2009): 57-65.

[4] Chen, S.C.; Tu, G.C.; Hung, C.Y.; Huang, C.A.; and Rei, M.H. Preparation of palladium membrane by electroplating on AISI 316Lporous stainless steel supports and its use form ethanol steam reformer **Journal of Membrane Science** 314 (2008): 5-14.

[5] Ma, Y.H.; Engwall, E.E.; and Mardilovich, I.P. Composite palladium and palladium-alloy membranes for high temperature hydrogen separations **Fuel Chemistry Division Preprints** 48(1) (2003): 333-334.

[6] Ryi, S.K.; et al. Characterization of Pd-Cu-Ni ternary alloy membrane prepared by magnetron sputtering and Cu-reflow on porous nickel support for hydrogen separation. **Separation and Purification Technology** 50 (2006): 82-91.

[7] Knapton, A.G. Palladium Alloys for Hydrogen Diffusion Membranes A REVIEW OF HIGH PERMEABILITY MATERIALS. **Platinum Metals Review** 21 (1977): 44-50.

[8] Bruce, R.L.; Omar, I.; Way, J.D.; David, E.; and Kent, C. Un-supported Palladium Alloy Membranes for the Production of Hydrogen. **Inorganic Membranes for Energy and Environmental Applications** 164 (2009): 203-219.

[9]   Bosko, M.L.; et al. Characterization of Pd-Ag membranes after exposure to hydrogen flux at high temperatures **Journal of Membrane Science** 306 (2007): 56-65.

[10] Phair, J.W.; and Badwal, S.P.S. Materials for separation membranes in hydrogen and oxygen production and future power generation **Science and Technology of Advanced Materials** 7 (2006): 792-805.

[11] Gupta R.B. **Hydrogen fuel: production, transport, and storage CRC Press**, 2008.

[12] **Hydrogen separation** [Online]. 2008 Available from: http://www.aist.go.jp/aist_e/aist_today/2008_29/feature/feature_03.html[2010, Febuary21]

[13] Uemiya, S.; Sato, N.; Ando, H.; Kude, Y.; Matsuda, T.**;** and Kikuchi, K. Separation of hydrogen through palladium thin film supported on a porous glass tube Shigeyuki **Journal of Membrane Science** 56 (1991): 303-313.

[14] Ma, Y.H. Composite Pd and Pd/Alloy Membranes. **Inorganic Membranes for Energy and Environmental Applications** (2008): 241-254.

[15] Bruce, R.L.; Omar, I.; Way, J.D.; David, E.; and Kent, C. Un-supported palladium alloy membranes for the production of hydrogen. **Inorganic Membranes for Energy and Environmental Applications** (2009): 203-219.

[16] Bernardo, P.; Drioli, E.; and Golemme, G. Membrane Gas Separation: A Review *Ind. Eng. Chem.* **Res.** 48 (2009): 4638-4663.

[17] Akis B.C.; Datta, R.; and Ma, Y.H. Preparation of Pd-Ag/PSS composite membranes for hydrogen separation **Chemical Engineering** (2004): 1-132.

[18] **Diffusion: the Phenomena (1) (Interdiffusion)** [Online]. 2006 Available from:http://www.fen.bilkent.edu.tr/~bengu/chem201/FinalCourseNotes/Chapter_05_avi_erman.ppt [2010, March 1]

[19] **Diffusion in Solids** [Online]. 2005 Available from:
http://dmseg5.case.edu/classes/emse201/overheads/Diffusio1.pdf
[2010, March 1]

[20] **Diffusion** [Online]. 2005 Available from: http://www.matsceng.ohio-state.edu/mse205/lectures/chapter5/chap5.pdf [2010, March1]

[21] **Non-steady State Diffusion** [Online]. 2005 Available from:
http://www.matsceng.ohiostate.edu/mse205/lectures/chapter5/chap5.pdf [2010, March1]

[22] **Metal plating** [Online]. 2009 Available from:
http://www.themetalcasting.com/metal-plating.html [2010, September10]

[23] Chalmers, B. **Physical Metallurgy** New York: John Wiley and Sons, 1959.

[24] Ryi, S.K.; et al. A new membrane module design with disc geometry for the separation of hydrogen using Pd alloy membranes **Journal of Membrane Science** 297 (2007): 217-225.

[25] Omayma, A.G.; Abou Tabl, M.H.; Abdel Hamid, Z.; Mostafa, S.F., Electroplating of chromium and Cr-carbide coating for carbon fiber. **Surface & coating Technology** 201 (2006): 1357-1362.

[26] **Electroless plating** [Online]. 2009 Available from:
http://composite.about.com/library/glossary/e/bldef-e1925.htm
[2010, August24]

[27] Notis, M.R.; Brown, J.; Zedalis S.M. and Brugger**,** T. **Alloy Phase Diagrams** ASM International Alloy Phase Diagram, 1992.

[28] Sidney, H. Avner **Introduction to Physical Metallurgy** New York: McGraw-Hill, 1964.

[29] Eero, S.; Hero H.A.; and Morten S. Phase equilibrium in Ag-Pd-Cu dental alloys. **Scandinavian Institute of Dental Materials**, 41 (1983): 363-368.

[30] Battye, S.H.M. **Metal for Engineering Craftsmen** London: Council for Small industries in Rural Area, 1979.

[31] Henish, H.; Roy, R.; and Cross, L.E. **Phase Transitions**, Pergamon, 1973.

[32] **X-Ray Diffraction (XRD)** [Online]. 2002 Available from:
http://prism.mit.edu/xray/BasicsofXRD.ppt [2010, March 1]

[33] Rointan, F.B. **Coatings Science, Technology and Applications** New Jersey:
Noyes Pubbilcation, 1994.

[34] Mario Birkholz. **Thin Film Analysis by X-Ray Scattering** Weinheim: Wiley-
Vch Verlag GmbH & Co., 2006.

[35] **Scanning Electron Microscopy (SEM) [**Online]. 2005 Available from:
https://wiki.usask.ca/bio_tech_doc/index.php/How_an_SEM_works
[2010, March1]

[36] Loretto, M.H. Electron Beam Analysis of Materials. London: Chapman & Hall,
1994.

[37] Anthony C. Fischer-Cripps. **Mechanical engineering series nanoindentation**.
New York: Spring-Verlag New York, LLC, 2004.

[38] Huo, D.; Liang, Y.; and Cheng, K.; An investigation of nanoindentation tests on
the single crystal copper thin film via an AFM and MD simulation.
Journal of Mechanical Engineering Science 221 (2007): 259-266.

[39] Peters, T.A.; Stange, M.; Klette, H. and Bredesen, R. High pressure
performance of thin Pd-23%Ag/stainless steel composite membranes
in water gas shift gas mixtures; influence of dilution, mass transfer
and surface effects on the hydrogen flux. **Journal of Membrane
Science** 316 (2008): 119-127.

[40] Gao, H.; Lin, J.Y.S.; Li, Y.; and Zhang, B. Electroless plating synthesis,
characterization and permeation properties of Pd-Cu membranes
supported on ZrO_2 modified porous stainless steel. **Journal of
Membrane Science** 265 (2005): 142-152.

[41] Lee, D.W.; Lee, Y.G.; Nam, S.E.; Ihm, S.K.; and Lee, K.H. Study on the
variation of morphology and separation behavior of the stainless steel
supported membranes at high temperature. **Journal of Membrane
Science** 220 (2003): 137-153.

[42] Wang, L.; Ryo,Y.; Shigeyuki, U.; Fabrication of novel Pd-Ag-Ru/Al_2O_3 ternary
alloy composite membrane with remarkably enhanced H_2
permeability. **Journal of Membrane Science** 306 (2007): 1-7.

[43] Ma, Y.H.; et al. Characterization of intermetallic diffusion barrier and alloy formation for Pd/Cu and Pd/Ag porous stainless steel composite membranes. **Industrial & Engineering Chemistry Research** 43 (**2004):** 2936-2945.

[44] Stefanov, P.; Stoychev, D.; Stoycheva, M.; and Marinova, Ts., XPS and SEM studies of chromium oxide films chemically formed on stainless steel 316L. **Materials Chemistry and Physics**, 65(**2000**): 212-215.

[45] Ma, Y.H.; Madilovich, I.P. and Engwall, E.E. Thin Composite Palladium and Palladium/Alloy **Membranes for Hydrogen Separation** 984 (2003): 346-360.

[46] Samandari, S.S.; and Gross, K.A.; Nanoindentation Reveals Mechanical Properties within Thermally Sprayed Hydroxyapatite Coatings. **Surface Coating Technology** 203 (2009): 1660-1664.

[47] Sabina, K. et al. The effects of fabrication and annealing on the structure and hydrogen permeation of Pd-Au binary alloy membranes. **Journal of Membrane Science** 340 (2009): 227-233.

[48] Cheng, Y.S. and Yeung, K.L. Effects of electroless plating chemistry on the synthesis of palladium membranes **Journal of Membrane Science** 182 (2001): 195-203

[49] Mardilovich, P.P.; She, Y., Rei, M.H. and Ma, Y.H. Defect free palladium membranes on porous stainless steel supports. **AIChE Journal** 44 (1998): 310-322.

[50] Ilias, S. Separation of Hydrogen and Carbon Dioxide Using a Novel Membrane Reactor in Advanced Fossil **Energy Conversion Process** (2005): 1-87.

[51] Tong, J.; Kashima, Y.; Shirai, R.; Suda, H. and Matsumura, Y. Thin Defect-free Pd membrane deposited on asymmetric porous stainless steel substrate. **Industrial & Engineering Chemistry Research** (2005): 44, 8025-8032.

[52] Stadlmayr, W. et al. Temperature-induced modifications of Pd-Zn layers on Pd(111) **Journal Physical Chemistry C** 114 (2010): 10850-10856.

[53] Henish, H.; Roy, R.; and Cross, L.E. **Phase Transitions**, Pergamon, 1973.

[54] Kim, J.Y.; Yu, J.; Lee, J.H. and Lee, T.Y. The Effects of Electroplating Parameters on the Composition and Morphology of Sn-Ag Solder. **Journal of Electronic Materials** 33 (2004): 1459-1464.

[55] Bosko, M.L.; Munera, J.F.; Lombardo, E.A. and Cornaglia, L.M. Dry reforming of methane in membrane reactors using Pd and Pd-Ag composite membranes on a NaA zeolite modified porous stainless steel support. **Journal of Membrane Science** 364 (2010): 17-26.

[56] Nair, R.; Choi, J.; Harold, M.P. Electroless plating and permeation features of Pd and Pd/Ag hollow fiber composite membranes. **Journal of Membrane Science** 288 (2007): 67-84.

[57] Kamakoti, P.; and Sholl, D.S.; Towards first principles-based identification of ternary alloys for hydrogen purification membranes. **Journal of Membrane Science** 279 (2006): 94-99.

[58] Tarditi**, A.M. and** Cornaglia**, L.M.** Novel PdAgCu ternary alloy as promising materials for hydrogen separation membranes: Synthesis and characterization Surface Science 605 (2011): 62-71.

[59] Paglieri, S. N. and Way, J. D. Innovations in palladium membrane research. **Separation and Purification Methods** 31(1) (2002): 1-169.

[60] Coulter, K. High Permeability Ternary palladium alloy membranes with improved sulfur and halide tolerance. **Southwest Research Institute** (2007): 110-113.

[61] Ryi, S.K.; Li, A.; Lim, C.J. and Grace, J.R. Novel non-alloy Ru/Pd composite membrane fabricated by electroless plating for hydrogen separation. **International of Hydrogen Energy** xxx (2010): 1-6.

APPENDICES

Appendix A

Materials, Equipments and Instruments

1. Materials used in this work

2. Porous and non-porous 316L stainless steel, Mott Corporation
3. Quartz wool, Alltech
4. Argon gas, 99.999%, Praxair
5. Nitrogen gas, 99.999%, Bangkok Industrial Gas
6. Helium gas, 99.99%, Bangkok Industrial Gas
7. Hydrogen gas 99.95%, Bangkok Industrial Gas

2. Chemicals used in this work

2.1 Chemicals for cleaning process

1. Detergent
2. Iso-propanol (C_3H_7OH), Carlo Erba
3. Sodium carbonate (Na_2CO_3), Carlo Erba
4. Sodium hydroxide (NaOH), Carlo Erba

2.2 Chemicals for surface activation

1. Tin (II) chloride dehydrate ($SnCl_2.2H_2O$), 98%, Carlo Erba
2. Hydrocloric (HCl, 37% concentrated), JT. Baker
3. Palladium (II) chloride ($PdCl_2$), 99.9%, Alfa Aesar

2.3 Chemicals for intermetallic diffusion barrier

1. Chromium trioxide (CrO_3), Carlo Erba
2. Sulfuric acid (H_2SO_4), 95-97%, Merck

2.4 Chemicals for electroless deposition

1. Tetra ammine palladium (II) chloride monohydrate ($Pd(NH_3)_4Cl_2.H_2O$), (98%), Alfa Aesar
2. Disodium ethylenediaminetetraacetrate (Na_2EDTA), 99.5%, Carlo Erba
3. Hydrazine anhydrous (N_2H_4), 99.5% , Aldrich

2.5 Chemicals for electroplate deposition

1. Copper (II) sulphate ($CuSO_4$), Univar
2. Silver nitrate ($AgNO_3$), Merck

3. Equipments used in this work

1. Furnace reactor, Lenton
2. Digital flow meter, Altech
3. Power supply, Mean well switching

4. Instruments used in this work

1. Scanning electron microscope (SEM), JEOL model JSM-5800LV with Energy Dispersive Spectrometer (EDS)
2. X-ray diffractometer (XRD), Rigaku Geigerflex X-ray diffractometer equipped with a CuK-radiation source
3. The nanoindentation tester (CSM instruments) at Metallurgy and Materials Science Research Institute, Chulalongkorn University

Appendix B

Hydrogen permeation test

1. Hydrogen flow rate of $Pd_{0.80}Ag_{0.05}Cu_{0.15}$ alloy membrane

Temp (°C)		Flow rate (mL/min) at different pressure (atm)					
		0.5	1.0	1.5	2.0	2.5	3.0
350°C	1	1.15	2.75	4.24	6.04	7.57	8.87
	2	1.16	2.78	4.23	6.04	7.55	8.87
	3	1.18	2.77	4.25	6.05	7.58	8.86
	Avg	1.17	2.76	4.24	6.04	7.57	8.87
	SD	0.01	0.01	0.01	0.005	0.01	0.005
400°C	1	1.33	3.15	4.73	6.38	7.92	9.41
	2	1.33	3.14	4.72	6.36	7.91	9.43
	3	1.34	3.12	4.70	6.40	7.94	9.44
	Avg	1.33	3.14	4.72	6.39	7.93	9.42
	SD	0.005	0.01	0.01	0.02	0.01	0.01
450°C	1	1.46	3.34	5.03	6.74	8.33	9.95
	2	1.44	3.35	5.02	6.73	8.34	9.94
	3	1.47	3.35	5.01	6.74	8.32	9.93
	Avg	1.46	3.35	5.02	6.74	8.33	9.94
	SD	0.01	0.005	0.01	0.005	0.01	0.01
500°C	1	1.52	3.42	5.23	6.94	8.64	10.36
	2	1.53	3.43	5.22	6.93	8.64	10.32
	3	1.51	3.43	5.23	6.94	8.63	10.34
	Avg	1.52	3.43	5.23	6.94	8.64	10.34
	SD	0.01	0.005	0.005	0.005	0.005	0.02

2. Hydrogen flow rate of $Pd_{0.85}Ag_{0.05}Cu_{0.10}$ alloy membrane

Temp (°C)		Flow rate (mL/min) at different pressure (atm)					
		0.5	1.0	1.5	2.0	2.5	3.0
350°C	1	0.62	1.67	2.99	4.18	5.53	7.11
	2	0.61	1.67	2.97	4.16	5.51	7.12
	3	0.63	1.66	2.98	4.19	5.52	7.13
	Avg	0.62	1.67	2.98	4.18	5.52	7.12
	SD	0.01	0.005	0.01	0.01	0.01	0.01
400°C	1	0.86	2.11	3.71	5.0	6.26	7.69
	2	0.88	2.12	3.71	5.01	6.24	7.66
	3	0.87	2.10	3.74	5.03	6.25	7.67
	Avg	0.87	2.11	3.72	5.02	6.25	7.69
	SD	0.01	0.01	0.01	0.01	0.01	0.01
450°C	1	0.96	2.35	4.09	5.46	6.83	8.38
	2	0.92	2.35	4.06	5.45	6.85	8.40
	3	0.94	2.32	4.07	5.43	6.86	8.38
	Avg	0.94	2.34	4.08	5.45	6.85	8.39
	SD	0.02	0.01	0.01	0.01	0.01	0.01
500°C	1	1.07	2.62	4.50	5.89	7.54	8.91
	2	1.08	2.63	4.51	5.86	7.52	8.93
	3	1.08	2.59	4.52	5.87	7.54	8.92
	Avg	1.08	2.61	4.51	5.88	7.53	8.92
	SD	0.005	0.02	0.01	0.01	0.01	0.01

3. Hydrogen flow rate of $Pd_{0.90}Ag_{0.05}Cu_{0.05}$ alloy membrane

Temperature (°C)		Flow rate (mL/min) at different pressure (atm)					
		0.5	1.0	1.5	2.0	2.5	3.0
350°C	1	0.62	1.66	2.98	4.17	5.52	6.83
	2	0.61	1.67	2.97	4.18	5.52	6.81
	3	0.62	1.67	2.98	4.18	5.52	6.82
	Avg	0.62	1.67	2.98	4.18	5.52	6.81
	SD	0.005	0.005	0.005	0.005	0.00	0.01
400°C	1	0.87	2.11	3.72	5.02	6.25	7.69
	2	0.86	2.12	3.72	5.01	6.26	7.68
	3	0.87	2.11	3.71	5.03	6.24	7.69
	Avg	0.87	2.11	3.72	5.02	6.25	7.69
	SD	0.005	0.005	0.005	0.01	0.01	0.005
450°C	1	0.94	2.34	4.09	5.45	6.87	8.38
	2	0.94	2.34	4.07	5.45	6.86	8.39
	3	0.93	2.34	4.08	5.45	6.84	8.39
	Avg	0.94	2.34	4.08	5.45	6.85	8.39
	SD	0.005	0.00	0.01	0.00	0.01	0.005
500°C	1	1.07	2.62	4.51	5.89	7.55	8.92
	2	1.08	2.61	4.52	5.87	7.52	8.91
	3	1.08	2.61	4.50	5.88	7.53	8.93
	Avg	1.08	2.61	4.51	5.88	7.53	8.92
	SD	0.005	0.005	0.01	0.01	0.01	0.01

4. Hydrogen flow rate of $Cr_2O_3/Pd_{0.85}Ag_{0.05}Cu_{0.010}$ alloy membrane

Temperature (°C)		Flow rate (mL/min) at different pressure (atm)					
		0.5	1.0	1.5	2.0	2.5	3.0
350°C	1	1.47	3.47	5.16	6.92	8.82	11.32
	2	1.48	3.47	5.15	6.93	8.81	11.32
	3	1.49	3.48	5.16	6.92	8.83	11.32
	Avg	1.48	3.47	5.16	6.92	8.82	11.32
	SD	0.01	0.005	0.005	0.005	0.01	0.00
400°C	1	1.69	3.76	5.74	7.67	9.83	11.75
	2	1.68	3.76	5.72	7.65	9.82	11.74
	3	1.68	3.77	5.73	7.66	9.81	11.74
	Avg	1.68	3.76	5.73	7.66	9.82	11.74
	SD	0.005	0.005	0.01	0.01	0.01	0.005
450°C	1	1.87	4.15	5.98	8.11	10.51	12.57
	2	1.87	4.17	5.97	8.12	10.53	12.56
	3	1.86	4.16	5.96	8.11	10.52	12.57
	Avg	1.87	4.17	5.97	8.11	10.52	12.57
	SD	0.005	0.01	0.01	0.005	0.00	0.005
500°C	1	2.17	4.31	6.60	8.78	10.98	12.85
	2	2.18	4.34	6.58	8.76	10.97	12.84
	3	2.19	4.35	6.56	8.77	10.96	12.83
	Avg	2.18	4.33	6.58	8.77	10.97	12.83
	SD	0.01	0.02	0.02	0.01	0.01	0.01

5. Hydrogen flow rate of $Pd_{0.60}Cu_{0.40}$ alloy membrane

Temp (°C)	No barrier	Flow rate (mL/min) at different pressure (atm)					
		0.5	1.0	1.5	2.0	2.5	3.0
350°C	1	1.13	2.63	3.79	5.09	6.52	7.67
	2	1.15	2.61	3.80	5.09	6.50	7.66
	3	1.14	2.58	3.84	5.08	6.53	7.63
	Avg	1.14	2.60	3.82	5.09	6.51	7.64
	SD	0.01	0.03	0.02	0.005	0.01	0.02
400°C	1	1.43	3.07	4.33	5.43	6.83	7.93
	2	1.44	3.09	4.36	5.44	6.76	7.92
	3	1.41	3.04	4.34	5.46	6.80	7.95
	Avg	1.42	3.06	4.35	5.44	6.80	7.94
	SD	0.01	0.02	0.01	0.01	0.03	0.02
450°C	1	1.82	3.50	4.66	5.72	7.14	8.25
	2	1.84	3.50	4.67	5.74	7.15	8.22
	3	1.79	3.52	4.67	5.70	7.13	8.28
	Avg	1.82	3.51	4.67	5.72	7.14	8.25
	SD	0.02	0.01	0.005	0.02	0.01	0.03
500°C	1	2.04	3.74	5.11	6.22	7.44	8.47
	2	2.08	3.70	5.10	6.15	7.45	8.47
	3	2.02	3.72	5.12	6.19	7.47	8.47
	Avg	2.05	3.72	5.11	6.19	7.46	8.47
	SD	0.03	0.02	0.01	0.03	0.02	0.00

ศูนย์วิทยทรัพยากร

จุฬาลงกรณ์มหาวิทยาลัย

6. Hydrogen flow rate of $Pd_{0.70}Ag_{0.30}$ alloy membrane

Temp (°C)	No barrier	Flow rate (mL/min) at different pressure (atm)					
		0.5	1.0	1.5	2.0	2.5	3.0
350°C	1	1.12	2.62	3.91	4.93	6.42	7.55
	2	1.20	2.57	3.92	4.94	6.43	7.53
	3	1.09	2.59	3.94	4.95	6.39	7.54
	Avg	1.12	2.59	3.92	4.94	6.41	7.54
	SD	0.05	0.03	0.01	0.01	0.02	0.01
400°C	1	1.43	2.92	4.11	5.36	6.76	7.84
	2	1.41	2.94	4.12	5.35	6.75	7.84
	3	1.42	2.93	4.09	5.34	6.77	7.84
	Avg	1.42	2.93	4.10	5.35	6.76	7.84
	SD	0.01	0.01	0.01	0.01	0.01	7.84
450°C	1	1.64	3.26	4.41	5.88	7.13	8.12
	2	1.62	3.25	4.43	5.83	7.12	8.16
	3	1.67	3.28	4.40	5.83	7.15	8.14
	Avg	1.64	3.27	4.41	5.84	7.14	8.15
	SD	0.02	0.01	0.01	0.02	0.01	0.02
500°C	1	1.83	3.62	4.82	6.21	7.45	8.38
	2	1.85	3.60	4.78	6.19	7.47	8.37
	3	1.86	3.61	4.80	6.15	7.46	8.36
	Avg	1.86	3.61	4.81	6.19	7.46	8.37
	SD	0.01	0.01	0.02	0.03	0.01	0.01

7. **Hydrogen flow rate of Pd membrane**

Temp (°C)	No barrier	Flow rate (mL/min) at different pressure (atm)					
		0.5	1.0	1.5	2.0	2.5	3.0
350°C	1	0.68	1.83	3.12	4.11	5.23	6.21
	2	0.69	1.84	3.09	4.12	5.26	6.22
	3	0.67	1.83	3.10	4.13	5.23	6.20
	Avg	0.68	1.84	3.10	4.12	5.24	6.21
	SD	0.01	0.005	0.01	0.01	0.03	0.01
400°C	1	1.00	2.37	3.59	5.05	6.15	7.13
	2	0.98	2.36	3.59	5.09	6.17	7.14
	3	0.95	2.32	3.60	5.03	6.04	7.12
	Avg	0.98	2.35	3.59	5.06	6.12	7.13
	SD	0.02	0.02	0.005	0.03	0.07	0.06
450°C	1	1.03	2.66	4.13	5.24	6.14	7.43
	2	1.01	2.68	4.17	5.24	6.12	7.42
	3	1.00	2.64	4.11	5.18	6.19	7.44
	Avg	1.02	2.66	4.14	5.22	6.15	7.43
	SD	0.01	0.02	0.03	0.03	0.03	0.01
500°C	1	1.33	2.89	4.14	5.24	6.68	7.83
	2	1.35	2.83	4.16	5.31	6.64	7.94
	3	1.33	2.86	4.10	5.26	6.63	7.91
	Avg	1.33	2.86	4.12	5.27	6.65	7.93
	SD	0.01	0.03	0.04	0.03	0.02	0.05

8. Hydrogen flux of Pd-based membranes

Membrane	Temp (°C)	*Flux (m^3/m^2h) at $P_{HP}^{1/2} - P_{LP}^{1/2}$					
		0.707	1	1.125	1.414	1.581	1.732
$Pd_{0.80}Ag_{0.05}Cu_{0.15}$	350°C	0.58	1.35	2.12	2.86	3.65	4.30
	400°C	0.64	1.45	2.26	3.06	3.84	4.58
	450°C	0.69	1.62	2.39	3.25	4.00	4.70
	500°C	0.74	1.71	2.59	3.38	4.14	4.91
$Pd_{0.85}Ag_{0.05}Cu_{0.10}$	350°C	0.58	1.45	2.23	3.03	3.78	4.45
	400°C	0.66	1.63	2.42	3.21	3.98	4.73
	450°C	0.73	1.68	2.52	3.38	4.18	5.03
	500°C	0.76	1.72	2.57	3.48	4.28	5.29
$Pd_{0.90}Ag_{0.05}Cu_{0.05}$	350°C	0.31	0.88	1.49	2.19	2.77	3.46
	400°C	0.43	1.16	1.87	2.52	3.13	3.76
	450°C	0.47	1.17	1.98	2.74	3.43	4.21
	500°C	0.54	1.42	2.15	2.95	3.70	4.48
$Cr_2O_3/Pd_{0.85}Ag_{0.05}Cu_{0.15}$	350°C	0.74	1.74	2.59	3.49	4.43	5.68
	400°C	0.84	1.88	2.88	3.84	4.93	5.89
	450°C	0.93	2.09	2.99	4.07	5.28	6.21
	500°C	1.09	2.17	3.20	4.40	5.50	6.44
$Pd_{0.60}Cu_{0.40}$	350°C	0.57	1.31	1.92	2.55	3.27	3.83
	400°C	0.68	1.44	2.08	2.73	3.42	3.99
	450°C	0.71	1.46	2.15	2.87	3.58	4.14
	500°C	1.03	1.67	2.37	3.11	3.75	4.25
$Pd_{0.70}Ag_{0.30}$	350°C	0.36	0.84	1.26	1.71	2.21	2.72
	400°C	0.41	0.91	1.41	1.88	2.40	2.93
	450°C	0.45	1.02	1.46	2.00	2.58	3.08
	500°C	0.53	1.11	1.61	2.15	2.69	3.19
Pd	350°C	0.29	0.62	1.03	1.40	1.78	2.11
	400°C	0.44	0.76	1.09	1.46	1.84	2.11
	450°C	0.54	0.87	1.27	1.61	1.91	2.28
	500°C	0.63	1.00	1.34	1.68	1.99	2.27

* H_2 permeation flux (m^3/m^2h) = (flow rate of H_2 (mL/min)/active surface area) x 0.6

Active surface area = $3.14R^2$ (surface area of membrane disk) – $3.14r^2$ (surface area of graphite gasket)

$$= (3.14*0.625 \text{ cm}*0.625 \text{ cm}) - (3.14*0.1 \text{ cm}*0.1\text{cm})$$

$$= 1.195$$

VITAE

Miss Warunporn Pattarateeranon was born on June 2, 1985 in Samutsongkram, Thailand. She graduated with a Bachelor's degree of Science, Faculty of Science, Prince of Kingmongkut Thonburi University in 2008. She has continued her study in Master's degree, majoring in Petrochemistry and Polymer Science, Faculty of Science, Chulalongkorn University, Bangkok, Thailand since 2008 and finished her study in 2010.

Conference presentations

Pattarateeranon, **W.** Tungasmita S. and Tuntayanon. S., "Preparation of Pd-Cu alloy membrane on 316L stainless steel for hydrogen separation", The Sixth Thailand Materials Science and Technology Conference (M-SAT6), August 26-27, 2010 Bangkok, Thailand (Poster Presentation).*best poster award

Pattarateeranon, **W.** Tungasmita S. and Tuntayanon. S., "The fabrication of Pd-Ag and Pd-Ag-Cu alloy membranes for hydrogen separation", The 6th Mathematics and Physical Science Graduate Congress 2010 (6th MPSGC) December 13-15, 2010 Kuala Lumpur, Malaysia (Poster Presentation).
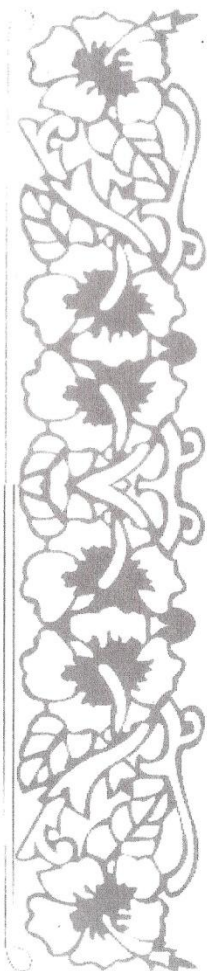
UNIVERSITY OF MALAYA

The Leader in Research & Innovation

CERTIFICATE OF PARTICIPATION

This certificate is awarded to

Ms. Pattarateeranon Warunporn

for participating in the

6th Mathematics and Physical Sciences Graduate Congress 2010

at Faculty of Science, University of Malaya
on 13th – 15th December 2010

In collaboration with

Chulalongkorn University

NUS National University of Singapore

Professor Dato' Dr. Mohd Sofian Azirun
Dean, Faculty of Science, University of Malaya